

Research Article

Zircon U-Pb geochronology and Sr-Nd-O isotopic constraints on the petrogenesis of the Jálama pluton (Central Iberian Zone, Spain)

Alfonso Pesquera ^{a,*}, Pilar Montero ^b, Pedro P. Gil-Crespo ^a^a Dpto. de Geología, Universidad del País Vasco (UPV/EHU), Campus de Bizkaia, Sarriena s/n, 48940 Leioa, Bizkaia, Spain^b Dpto. de Mineralogía y Petrología, Universidad de Granada Campus Fuentenueva, 18002 Granada, Spain

ARTICLE INFO

Article history:

Received 23 September 2020

Received in revised form 9 December 2020

Accepted 16 January 2021

Available online 23 January 2021

Keywords:

Zircon U-Pb geochronology

Sr-Nd-O isotopic data

Jálama pluton

ABSTRACT

In this paper we report a combined zircon U-Pb-O isotopes and bulk-rock Sr-Nd-O isotopes study on granitic rocks from the Jálama pluton, Central Iberian Zone. Zircon U-Pb ages of representative granitic rock samples are bracketed in the range of $306\text{--}304 \pm 3$ Ma, but within the level 2σ errors of U-Pb ages. Therefore it is not possible to establish differences in intrusion ages between the main granitic units that make up the Jálama pluton. Microgranular enclaves appear to be slightly older (309 ± 2 Ma), but they do overlap with the age of the granitic rocks. Sr-Nd isotopic data for enclaves of tonalitic composition preclude a simple mantle or crustal origin, but high mean zircon $\delta^{18}\text{O}$ values of $8.65 \pm 0.9\text{\textperthousand}$ and $\delta^{18}\text{O(WR)}$ values of $9.96\text{--}10.56\text{\textperthousand}$ reflect a largely crustally contaminated magma. The combination of field relations, petrography, bulk-rock geochemistry, Sr-Nd-O isotopic data, zircon $\delta^{18}\text{O}$ values and U-Pb ages provide compelling evidence that the granites from the Jálama pluton: (i) were coevally formed involving assimilation and mingling/mixing concomitant to fractional crystallization; and (ii) represent typical S-type granites that evolved from a same crustal source, potentially metasedimentary rocks from the Schist Greywacke Complex by considering the Neoproterozoic ages of the inherited zircons.

Published by Elsevier B.V.

1. Introduction

The Jálama pluton (JP) is a granitic body that outcrops in low-grade metasedimentary rocks of the Schist-Greywacke Complex (SGC), within the South Central Iberian Zone (CIZ) very close to the border with Portugal (Fig. 1). The CIZ constitutes the central domain of the Iberian Variscan belt (Fig. 1), the westernmost segment of the European Variscides, and represents a section of the Gondwana margin with a complex geological history from the Neoproterozoic to the Carboniferous (e.g., Martínez Catalán et al., 2014; Pereira et al., 2012).

The SGC is largely exposed in the southern domain of the Central Iberian zone, and consists of a very thick psammopelitic sequence of Neoproterozoic to lower Cambrian age with minor conglomerate, carbonate, and volcanoclastic layers. This siliciclastic sequence was interpreted to be deposited in an evolutive environment of arc-related basins near the north Gondwana active margin (Pereira et al., 2012; Villaseca et al., 2014). At some areas of the CIZ an Ordovician clastic sequence unconformably overlies Cambrian or Upper Proterozoic rocks.

The Variscan deformation can be summarized as follows: (1) Crustal thickening provoked by the continental collision between Laurussia and Gondwana during the late Paleozoic accompanied by folding and thrusting (D_1). Large scale folds with subvertical axial planes and a pervasive axial

planar foliation (S_1) were developed during this deformation. (2) D_1 structures are variably overprinted by D_2 deformation concomitant to the intra-orogenic extensional collapse, which is responsible for low-angle extensional shear zones and recumbent folds with sub-horizontal penetrative foliation (Diez Balda et al., 1995). (3) Later deformations affected the previous structures with the development of vertical to steeply-inclined strike-slip shear zones (Martínez Catalán et al., 2014). During the D_1 and D_2 , deformations a regional low- to high-grade metamorphism developed, which evolved from intermediate to low pressure conditions, reaching partial melting in the lower structural domains (Escuder Viruete et al., 2004).

The CIZ is characterized by a huge volume of igneous rocks related mainly to the Variscan orogeny. Strongly peraluminous granitoids (A/CNK ratios ≥ 1.1) with a crustal isotopic composition are more abundant than metaluminous granitoids and basic rocks (Bea, 2004; Villaseca et al., 1998). The JP has been considered to form part of the cordierite-monzogranite suite (Corretgé et al., 2004) or the S_2 granitoids of Villaseca (2011). However, it does not have cordierite like other S_2 granitoids in the CIZ; for example, those from the Guarda-Sabugal area (Neiva et al., 2011). The cordierite-monzogranite suite is also known as "Serie Mixta" in the literature, owing to the granitoids of this suite have intermediate characteristics between peraluminous leucogranites and granodiorites (Corretgé et al., 2004). Most granites of this group are confined in

* Corresponding author.

E-mail addresses: alfonso.pesquera@ehu.eus (A. Pesquera), pmontero@ugr.es (P. Montero), pedro.gil@ehu.eus (P.P. Gil-Crespo).

the southern domain of the CIZ, where they occur as epizonal zoned bodies intruding into the SGC; for example, in addition to the JP, the plutons of Castelo Branco, Nisa-Alburquerque, Cabeza de Araya, Central Extremadura batholith and Campanario-La Haba (Fig. 1). These granitoids are late-tectonic with respect to the main Variscan deformation phases, and share the following features (Table 1): (i) they form part of epizonal, zoned plutons; (ii) common presence of K-feldspar megacrysts; (iii) metasedimentary xenoliths and microgranular enclaves; (iv) mineral assemblages including biotite + muscovite ± cordierite ± tourmaline ± andalusite/sillimanite; (v) bulk-rock compositions with peraluminous character ($A/CNK \geq 1.1$), low CaO contents and relatively rich in P, which are consistent with the compositions of experimental melts derived from pelitic metasediments (e.g., Patiño Douce and Johnston, 1991); (vi) $^{87}\text{Sr}/^{86}\text{Sr}_{300} = 0.706\text{--}0.718$ and ϵNd_{300} between -2 and -6; (vii) available U-Pb and Rb-Sr ages of about 300–310 Ma; and (viii) associated aplites and pegmatites, some Li-rich (Antunes et al., 2008; Castro et al., 1999; Corretgé et al., 1985; Pereira et al., 2018; Roda-Robles et al., 2018; Solá et al., 2009; Villaseca et al., 2008).

This study builds upon the previous work of Pesquera et al. (2018) on the Jálama pluton. In this paper, we integrate detailed field observations, petrographic and mineralogical data, bulk-rock geochemistry, together with Sr-Nd-O isotopic data and zircon U-Pb geochronology, in order to understand the processes involved in its genesis. With this series of data we will intend to constrain the possible magma sources, and explore implications for the Variscan magmatism in the CIZ.

2. Petrography and bulk-rock chemistry

The JP has sharp but irregular intrusive contacts with low-grade metasedimentary rocks from the SGC, with an elongation roughly

parallel to the regional foliation (Fig. 1). A contact metamorphism with the formation of cordierite is developed around the intrusion, indicating low-pressure conditions. Modal proportions are typical of monzogranites from the “Serie Mixta” (Fig. 2). The JP can be subdivided into three major units based on petrographic characteristics, mineral associations and modal estimates (Table 2). The Hoyos unit (HS) is a two-mica ± sillimanite monzogranite, fine- to coarse-grained and porphyritic tendency, that outcrops in the central part (Fig. 1). The San Martín de Trevejo unit (SMT) is a two-mica ± tourmaline monzogranite, without sillimanite, and it is the one with the largest extension on the pluton (Fig. 1). It shows a seriate to porphyritic texture with K-feldspar megacrysts up to ~10 cm in length, particularly in the southern part of the pluton. The contact between the HS and SMT units is gradational (Fig. 3a), with mingling processes at some locations. Modal mineral layering where layers are millimeter to centimeter thick, lens- to sheet shaped, and most apparent by the contrasting amounts of biotite or feldspar megacrysts, is observed in places (Fig. 3b). Locally biotite-rich schlieren can also be observed, particularly near ellipsoidal microgranular enclaves following the directional fabric of the rock defined by feldspar megacrysts. The Valverde del Fresno unit (VF) is a fine- to medium-grained leucogranite with muscovite and tourmaline, which represents a narrow discontinuous band in the northern margin of the pluton (Fig. 1).

The monzogranites show locally microgranular enclaves and metasedimentary xenoliths. The microgranular enclaves are typically fine-grained with a tonalitic to granodioritic composition (Figs. 3c, d, e). They are mainly composed of plagioclase phenocrysts and laths displaying complex zoning, biotite ± amphibole, muscovite (absent in tonalites), interstitial K-feldspar, and quartz. Apatite, zircon, ilmenite, Fe-Cu sulphides and titanite are the main accessory minerals. The

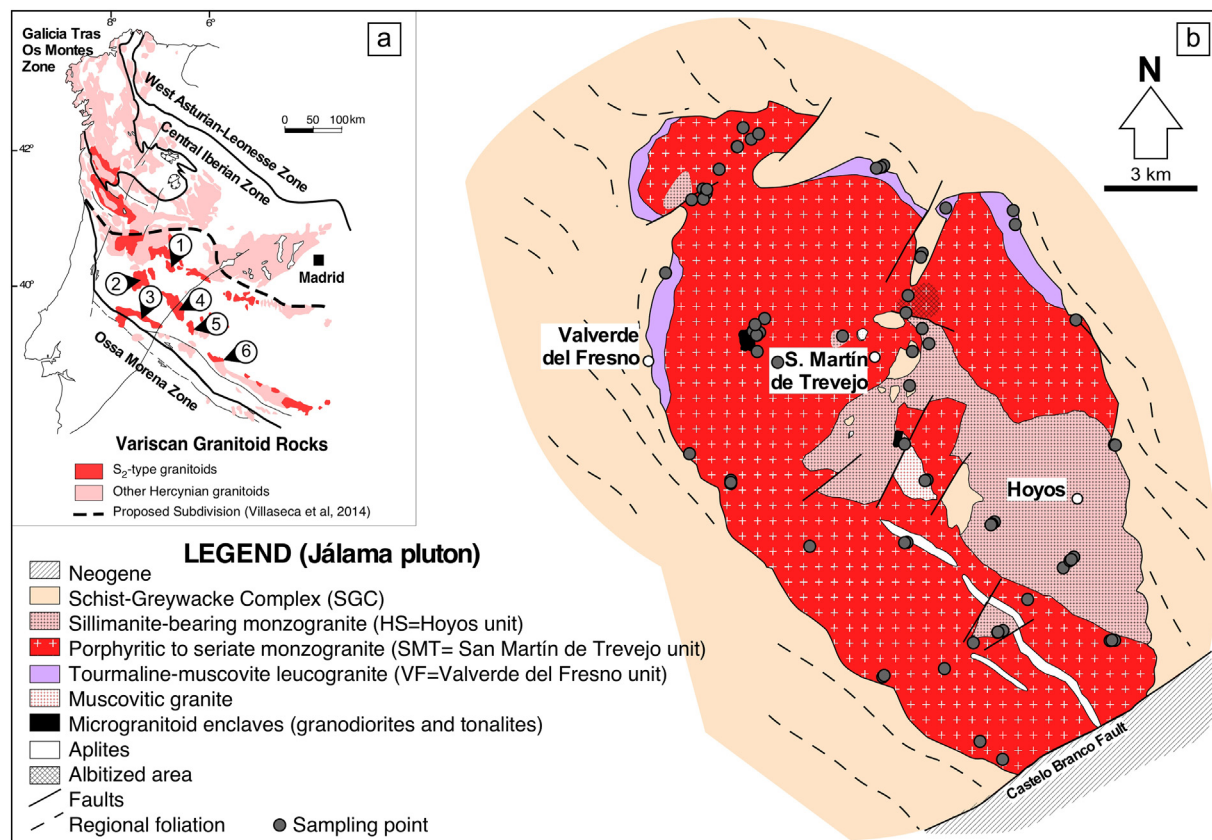


Fig. 1. (a) Map showing the Jálama area and the distribution of Variscan granitoids in the Central Iberian Zone. (b) Simplified geological map of the Jálama pluton and its host rocks (modified from Ugidos et al., 1984; García de Figuerola et al., 1988a, 1988b; Ramírez, 1996). Representative granitoids of the “Serie Mixta”: (1) Jálama; (2) Castelo Branco; (3) Alburquerque; (4) Cabeza de Araya; (5) Central Extremadura Batholith; and (6) Campanario-La Haba.

Table 1

General characteristics of the Jálama pluton compared to other granitoids from the “Serie Mixta” (Antunes et al., 2008; Corretgé et al., 1985, 2004; Pereira et al., 2018)

Granitoid	Rock-types	Enclaves	Mineral association	Geochemical classification	Geochronological data
Jálama	Monzogranites	Microgranular	Qtz+Kfs+Pl+Bt+Ms	Peraluminous	305–309 Ma SHRIMS U-Pb zircon
	Leucogranites	Metasedimentary	±Tur±Sil	Ferroan	
	Aplites and pegmatites			Alkali-calcic to calc-alkalic	
Castelo Branco	Monzogranites	Microgranular	Qtz+Kfs+Pl+Bt+Ms	Peraluminous	310 Ma
	Leucogranites	Metasedimentary	±Tur±And±Sil±Crd	Ferroan	ID-TIMS zircon
	Aplites and pegmatites			Alkali-calcic	
Cabeza de Araya	Monzogranites	Microgranular	Qtz+Kfs+Pl+Bt+Ms±Crd±Tur±And±Sil	Peraluminous	305–308 Ma
	Leucogranites	Metasedimentary		Ferroan to magnesian	SHRIMS U-Pb zircon
	Aplites and pegmatites			Alkali-calcic	
CBEX	Monzogranites	Microgranular	Qtz+Kfs+Pl+Bt+Ms±Crd±Tur±And±Sil	Peraluminous	309 Ma
	Leucogranites	Metasedimentary		Magnesian	SHRIMS U-Pb zircon
	Aplites and pegmatites				

microgranular enclaves exhibit different shapes, from angular fragments to ellipsoidal or rounded bodies (Fig. 3c), and the contacts with the felsic host vary from almost linear to strongly irregular and gradational. Locally, they appear as pillow-like with crenulate and chilled margins, and show evidence of spalling and net-veining by the host felsic magma (Fig. 3d). Hybrid facies with small dark to fuzzy inclusions, which represent the remnants of the more basic magmatic component, are found in places (Fig. 3e). Field evidence for mingling and mixing between microgranular enclaves and the granite host has been widely documented by Pesquera et al. (2018). Also, millimetre- to centimeter-sized metasedimentary xenoliths occur locally in the monzogranites, particularly in the Hoyos unit. They present a variable appearance, from fuzzy, partially digested xenoliths to discrete bodies showing sharp, subrounded or angular shapes with a clear foliation (Fig. 3f). On the other hand, pegmatitic segregations and veins, aplites, miarolitic cavities, and albited zones are relatively common in the northern part of the pluton and are indicative of an important activity of fluids during the late stages of magmatic evolution.

Average bulk-rock compositions of granitic rocks corresponding to the different units that make up the JP are shown in Table S1 (Suppl.). Full data, analytical methods and geochemical characteristics of the JP can be found in Pesquera et al. (2018). According to the classification scheme of Frost et al. (2001), the granitic rocks are mostly ferroan with an alkali-calcic to calc-alkalic trend (Fig. 4a, b) and a peraluminous

affinity (Fig. 4c). The microgranular enclaves show a compositional variation within the magnesian and alkali-calcic domains (Fig. 4a, b) with a metaluminous to peraluminous affinity (Fig. 4c).

Except for B, Li, Cs, Ta and Sn which are higher in SMT than HS, compositional differences between HS and SMT granites are subtle (Suppl. Table S1). As a whole, however, the granites define an evolutionary trend where TiO_2 , FeO, MgO, CaO, Zr, Sr, Ba, Y and REE decrease with the increase of SiO_2 , while Na_2O , P_2O_5 , Rb, Li, Cs and Ta increase, suggesting feldspar, biotite and accessory minerals fractionation (Suppl. Fig. S1). It should be noted the relatively high content of P_2O_5 with normative apatite, so that JP granites can be considered as per-phosphorous granites according to Bea et al. (1992). The chemical trends culminate with the VF leucogranites showing the lowest values of TiO_2 , $\text{MgO}/(\text{MgO} + \text{FeO})$, K/Rb , Nb/Ta and Zr/Hf , as well as the highest values of Na_2O , Li, Cs, B, F, Sn, W, Ta and Rb/Sr . Sn-Ta mineralizations are closely associated with this marginal unit. In general, the JP granites share many characteristics with other Sn-bearing granites of the CIZ (Corretgé et al., 2004; Teixeira et al., 2012), as well as some S-type granites of the European Variscides (Romer et al., 2012).

The plots of Th vs. LREE and Y vs. HREE show good correlations (Suppl. Fig. S1), suggesting the presence of monazite and xenotime in the granitic rocks, in addition to zircon and apatite. Geochemical differences between the host rocks and microgranular enclaves are reflected by their discontinuous evolutionary trends of bulk-rock major and trace elements with increasing SiO_2 on binary variation diagrams. Chondrite normalized REE patterns for the HS and SMT monzogranites are very similar, with variable degrees of fractionation ($\text{La/Lu}_N \approx 11–36$) and variable Eu negative anomalies ($\text{Eu/Eu}^* \approx 0.15–0.25$). Marginal leucogranites are relatively depleted in REE ($\Sigma\text{REE} < 30 \text{ ppm}$) and less fractionated ($(\text{La/Lu})_N < 7$) than the monzogranites. The ΣREE contents of MEEs vary in the range of 150 to 325 ppm, with $(\text{La/Lu})_N \approx 13–24$, and $(\text{Eu/Eu}^*) \approx 0.20–0.35$ (for more details, see Pesquera et al., 2018).

3. Samples and methods

Four samples representing the spectrum of granitoid lithology and field relations were selected for zircon U-Pb geochronology: (1) Fine-grained tonalite (JAL-15-26) included in the SMT unit, with plagioclase (44 vol%), biotite (24 vol%), amphibole (8 vol%), k-feldspar (4 vol%) and quartz (18 vol%); (2) Fine- to coarse-grained monzogranite (JAL-16-13) from the HS unit with quartz (30 vol%), k-feldspar (24 vol%), plagioclase (29 vol%), biotite (9 vol%) and muscovite (7 vol%) as essential components; (3) medium to very-coarse-grained monzogranite (JAL-16-2) from the SMT unit including mainly quartz (31 vol%), k-feldspar (25 vol%), plagioclase (26 vol%), biotite (10 vol%) and muscovite (6 vol%); and (4) fine to medium-grained tourmaline-bearing leucogranite (JAL-18-1) from the VF unit with quartz (29 vol%), K-feldspar (27 vol%), plagioclase (29 vol%), muscovite (12 vol%) and tourmaline (2 vol%).

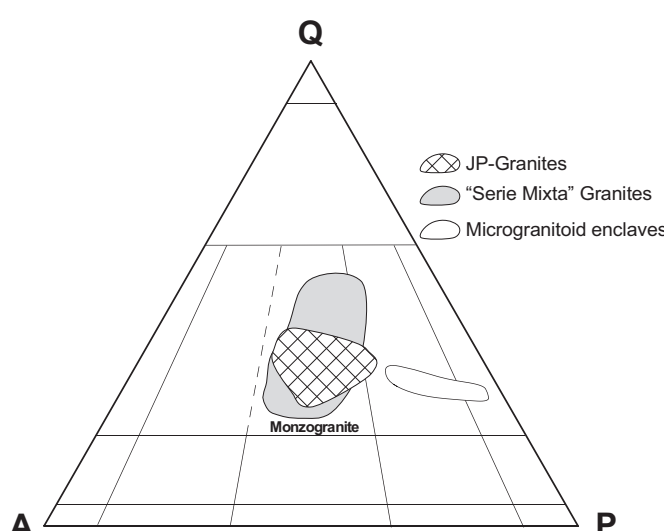


Fig. 2. Modal composition of the JP granites and microgranular enclaves in the QAP diagram of Le Bas and Streckeisen (1991), compared to that of SM granitoids.

Table 2

Petrographic characteristics of the main granite units recognized in the Jálama pluton.

Unit	Field relations	Mineral association and modal data (%)	Textural characteristics
HS Monzogranite	<ul style="list-style-type: none"> – Hypidiomorphic porphyritic to seriate texture – Fine to coarse-grained (usually < 2 cm) – Tendency for the minerals to be oriented – MM and MTS enclaves 	<p>Qtz (30), Kfs (23), Pl (29), Bt (10) > Ms (7) \pm Tur \pm Sil Ap, Ilm \pm Rt, Zrn, Mnz</p>	<ul style="list-style-type: none"> – Needles of Sil in Ms and Tur – Fine to medium-grained, subhedral Ms of primary character (> 0.6 wt% TiO₂) – Very fine- to fine-grained Ms replacing feldspars of secondary character – Euhedral to subhedral crystals of Kfs with Carlsbad and cross-hatched twinning – Perthitic intergrowths, Rapakivi and antirapakivi textures – Plagioclase (< 32% An) with variable zoning and different types of twinning – Myrmekites – Fine to medium-grained, subhedral Ms of primary character (> 0.6 wt% TiO₂) – Very fine- to fine-grained Ms replacing feldspars of secondary character – Euhedral to subhedral crystals of Kfs with Carlsbad and cross-hatched twinning – Oscillatory zoning in Kfs – Perthitic intergrowths, Rapakivi and antirapakivi textures – Plagioclase (< 30% An) with variable zoning and different types of twinning – Myrmekites – Anhedral to subhedral crystals of Tur with variable colour, commonly is closely associated with biotite – Symplectitic intergrowths of green tourmaline and feldspar – Abundant subhedral muscovite with Li₂O up to 0.39 wt% – Fine- to medium-grained, optically zoned, euhedral to subhedral crystals of Tur with a bluish-green to green colour – Unzoned or weakly zoned Pl (< 10 % An) – Perthitic Kfs with xenomorphic tendency
SMT Monzogranite	<ul style="list-style-type: none"> – Hypidiomorphic porphyritic to seriate texture – Medium to coarse-grained - Kfs megacrysts up to 10 cm, some of them with concentric zoning – Compositional layering – Tendency for the minerals to be oriented – MM enclaves 	<p>Qtz (32), Kfs (24), Pl (28), Bt (9) > Ms (6) \pm Tur Ap, Ilm \pm Rt, Zrn, Mnz</p>	
VF Leucogranite	<ul style="list-style-type: none"> – Xenomorphic to hypidiomorphic texture with equigranular tendency – Fine to medium-grained – Massive fabric 	<p>Qtz (27) + Kfs (27) + Pl (29) + Ms (12) \pm Tur (< 7%) \pm Bt (< 1%) Ap, Zrn, Mnz, Ilm \pm Rt \pm Cst</p>	

Zircons from these samples were separated by panning, using first water and then ethanol. The magnetic fraction was removed from the concentrates by using a Nd-magnet. Zircon grains were selected by handpicking under a binocular microscope and mounted on a 3.5 cm diameter epoxy SHRIMP megamount. Optical (transmitted and reflected light) and cathodoluminescence images were used to assess the zircons before their analysis. CL images were performed in a Zeiss SEM working at 10 kV with 1 nA as filament intensity and a spot size 520 μ m. Once coated with a 13 nm thick gold layer, U-Th-Pb analyses were made using a SHRIMP IIe/mc ion microprobe at the IBERSIMS laboratory of the CIC-University of Granada, Spain. The SHRIMP U-Th-Pb analytical method followed that described by Williams and Claeson (1987) and is described in detail on our laboratory website (www.ugr.es/~bersims). Analytical conditions can be resumed as follows: Raster time: 120 s, six scans per analysis, isotope peak sequence: ¹⁹⁶Zr₂O, ²⁰⁴Pb, ^{204.1}background, ²⁰⁶Pb, ²⁰⁷Pb, ²⁰⁸Pb, ²³⁸U, ²⁴⁸ThO, and ²⁵⁴UO, counting times per scan: 2 s for mass 196; 5 s for masses 238, 248, and 254; 15 s for masses 204, 206, and 208; and 20 s for mass 207. Uranium concentration calibrated using the SL13 reference zircon (Claoué-Long et al., 1995). U/Pb ratios were calibrated by means of the TEMORA-II reference zircon (417 Ma; Black et al., 2003), which was measured every 4 unknowns. All calibration procedures were performed with standards included on the same mount than samples. Mass calibration was performed with the home-made REG20 zircon standard (ca 2.5 Ga and high content of common lead). Data reduction was carried out with the SHRIMPTOOLS software (developed by F. Bea and downloadable from www.ugr.es/~fbea) using the STATA™ programming language.

Once analyzed U-Th-Pb, the megamounts were cleaned, re-polished, and coated with a 30 nm thick gold layer for oxygen isotope analyses following the method described by Ickert et al. (2008). Analytical conditions can be resumed as follows: the Cs gun set to yield a ~ 8 nA Cs + beam, the e-gun to neutralize Cs ions on non-conductive materials

set to an intensity of about 1 μ A, analyzed spots burned for about 5 min before measurements, secondary beam, and the e-gun fully optimized to maximize the ¹⁶O signal. Measurements were carried out in two sets of 10 scans each and 10 s per scan, so the real data collection time was 200 s per spot. The EISIE (electron-induced secondary ion emission) background was recorded during 10 s before and after each set, and subtracted from the ¹⁶O and ¹⁸O counts. TEMORA-II zircon was used as standard, measured every four unknowns, and cross-checked against the 91,500 zircon every 20 unknowns. The reproducibility of the standards was considered to be excellent: $\delta^{18}\text{O} = 8.17 \pm 0.34$ (2 σ) for the TEMORA-II and $\delta^{18}\text{O} = 9.98 \pm 0.26$ (2 σ) for the 91,500, respectively. Data reduction was made with the POXY program developed by P. Lanc and P. Holden at the Australian National University.

Isotope Sr and Nd analyses were performed at the Laboratory of Geochronology and isotope geology of the CIC-University of Granada (Spain). Samples were digested in a cleanroom using sub-boiling distillate ultraclean reagents and analyzed by thermal ionization mass spectrometry (TIMS) in a Finnigan Mat 262 spectrometer after chromatographic separation with ion-exchange resins in a cleanroom. Normalization values were ⁸⁶Sr/⁸⁸Sr = 0.1194 and ¹⁴⁶Nd/¹⁴⁴Nd = 0.7219. Blanks were 0.6 and 0.09 nanograms for Sr and Nd, respectively. The external precision (2 σ) was estimated from the last 10 replicates of the standard WS-E (Govindaraju et al., 1994), routinely analyzed each 10 unknown samples, and was better than 0.0013% for ⁸⁷Sr/⁸⁶Sr, and 0.0019% for ¹⁴³Nd/¹⁴⁴Nd. The internal precision was estimated based on the average of the standards NIST-987 for Sr with a mean ⁸⁷Sr/⁸⁶Sr = 0.710249 \pm 0.0003%, and Jndi-1 (Tanaka et al., 2000) for Nd with a mean ¹⁴³Nd/¹⁴⁴Nd = 0.512132 \pm 0.0005%. ⁸⁷Rb/⁸⁶Sr and ¹⁴⁷Sm/¹⁴⁴Nd ratios were directly determined by ICP-MS according to the method developed by Montero and Bea (1998), with a precision, estimated by analysing 10 replicates of the standard WS-E, better than 1.2% and 0.9% (2 σ) respectively.

Oxygen Isotopic analyses of bulk rock were performed in Actlabs (Activation Laboratories Ltd.) on a Finnigan MAT Delta, dual inlet,

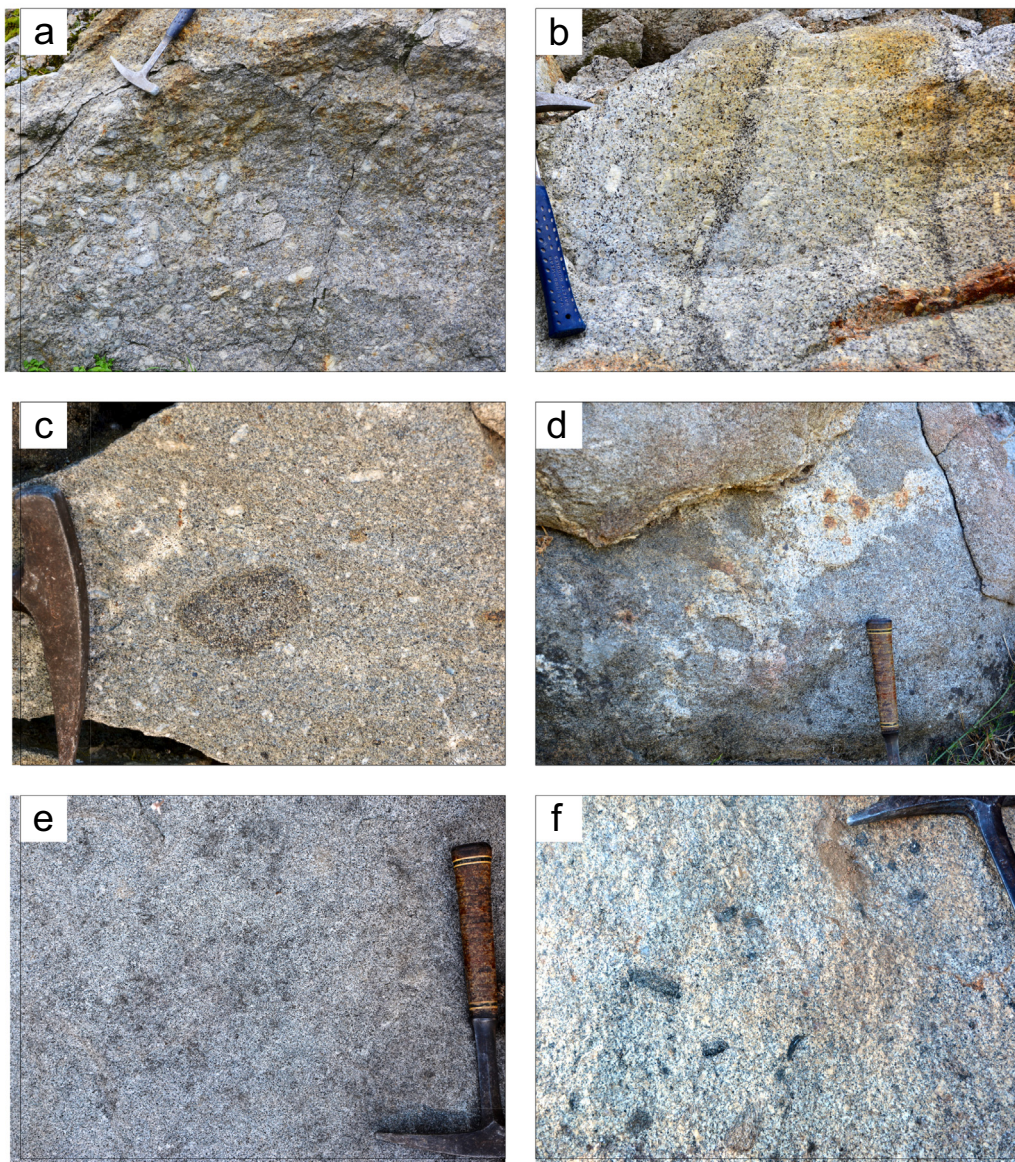


Fig. 3. Field examples of granitic rocks and enclaves in the JP: (a) Porphyritic monzogranite from the SMT unit in gradational contact with monzogranite from the HS (right side of the photo). Note the zonation of some feldspar megacrysts defined by gray rims and light gray to white cores. (b) Compositional layering in monzogranite defined by fine biotite-rich layers (< 3 cm thick) alternating with biotite-poor quartz-feldspar layers. Note the occurrence of feldspar megacrysts parallel to the layering. (c) Atoll-shaped microgranular enclave enclosed in heterogeneous hybrid granodiorite, showing leucocratic zones, K-feldspar megacrysts and films of felsic material. Note the presence of wispy schlieren and clots of fine-grained mafic material scattered by the rock. (d) Mingling/mixing between mafic rock and monzogranite with contacts varying from delicate to diffuse to sharp. Note the presence of partly fragmented pillows and veined by the monzogranite. The felsic member is relegated to an interlobe position, which injects into the mafic magma and disaggregates it with the development of hybrid zones. Small, surrounded more mafic globules includes into the enclaves can be also observed. (e) Hybrid rock consisting of dominantly fine grained granodioritic matrix with feldspar xenocrysts and darker irregular patches of tonalitic composition. (f) Monzogranite from the HS unit containing numerous metasedimentary xenoliths, some of them showing a high degree of digestion.

isotope ratio mass spectrometer. The data are reported in the standard delta notation as per mil deviations from V-SMOW. External reproducibility is $\pm 0.19\%$ (1σ) based on repeat analyses of the internal white crystal standard (WCS). The value for NBS 28 is $9.61 \pm 0.10\%$ (1σ).

4. Results

4.1. U-Pb zircon ages

In general, zircon occurs as stubby and subhedral to euhedral crystals with elongation ratios ranging mostly from 3 to 5 and variable size (normally $<200 \mu\text{m}$). The grains commonly show a combination of prismatic and pyramidal forms with a great variety of

microstructures, including inherited zircon grains, which can be observed in polished sections using a combination of high-resolution cathodoluminescence (CL) and transmitted light (TL) imaging. Inherited cores mostly of Neoproterozoic age can be recognized, apart from age, by different signs: surrounded shapes mantled by dark rims, truncate internal oscillatory zoning, and dark cores with microfractures starting at the margin of the core (Fig. 5).

Zircons from the tonalitic enclave are mainly long- to medium-prismatic, rarely rounded, with short pyramidal terminations and small to medium size (≈ 100 to $200 \mu\text{m}$ as average). In transmitted light, they are colorless or light brown to pinkish and always translucent. In CL they usually show a diffuse oscillatory zoning and also a zoning consisting of elongated bands along the main axis of the crystals. Convolute and patchy

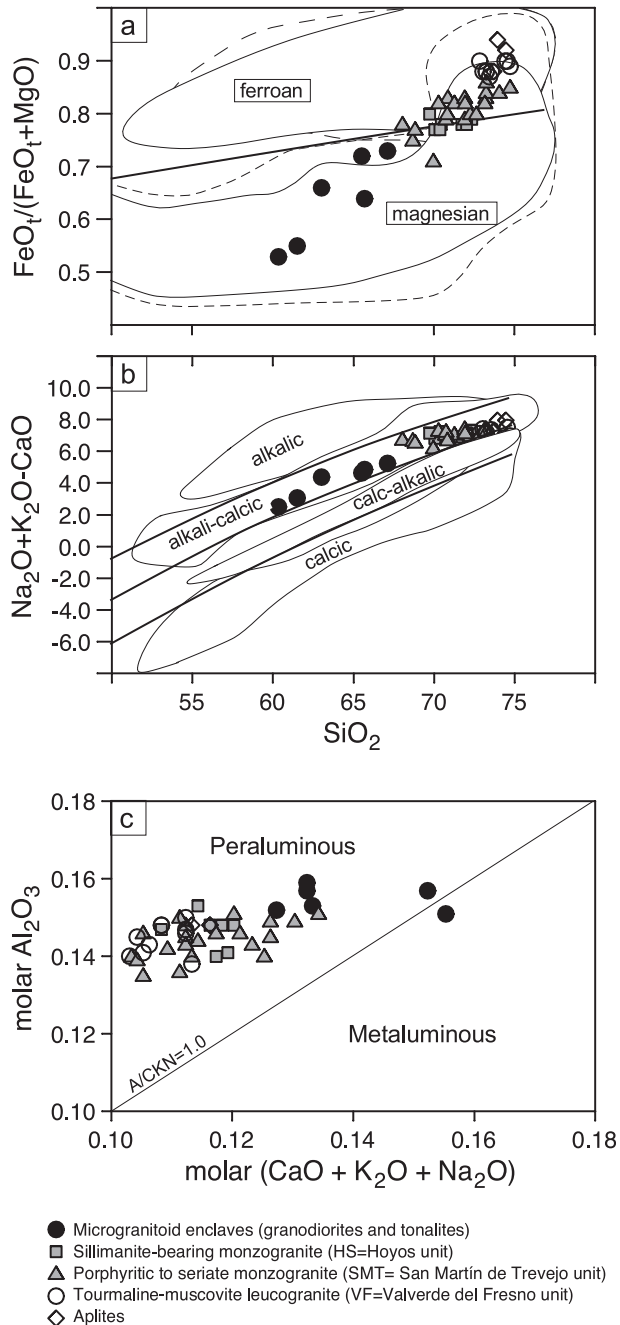


Fig. 4. (a) Fe-number (Frost et al., 2001) vs. wt% SiO₂. (b) MALI index (Frost et al., 2001) vs. wt% SiO₂. (c) Plot of molar (Na₂O + K₂O + CaO) vs. molar Al₂O₃ for samples of the Jálama pluton.

zoning are less common microstructures. In a few cases, internal parts of the grains appear darker, with no structure and rounded by discordantly zoned rims (Fig. 5a). Twenty four analyses have been performed in inner and outer parts of 24 grains, all of them are concordant or nearly concordant, with a discordance less than 6% (% discordance = [100 x (²⁰⁷Pb/²³⁵U age) - (²⁰⁶Pb/²³⁸U age)] / (²⁰⁷Pb/²³⁵U age)]. Twenty-three of these analyses plot in concordia defining a cluster yielding a weighted mean ²⁰⁶Pb/²³⁸U age of 309 ± 2 Ma (MSWD = 0.8) (Fig. 6a), which is considered the age of crystallization of the rock. One analysis yielded a ²⁰⁶Pb/²³⁸U age of 686 Ma, performed in a restitic crystal, morphologically different to the rest (Fig. 6a). Zircons from this rock have moderate U and Th contents (average = 308 and 177 ppm, respectively) and Th/U ratios in the range of 0.1–1.9 and an average of 0.6 (Suppl. Table S2).

Zircons from the sillimanite-bearing monzogranite (HS) are commonly elongated prismatic with short pyramidal forms, colorless or very light-colored, and an average size of about 200 µm. Light brown oval or rounded crystals, usually smaller, with an average size of about 100 µm are also observed. Small rounded inclusions along the elongation of crystals are not rare. In CL zircons show different microstructures (Fig. 5b): (i) relatively large crystals, highly cathodoluminescent, with diffuse oscillatory zoning or alternating longitudinal bands; (ii) low cathodoluminescent, completely black crystals without internal microstructures; and (iii) crystals with complex internal microstructure, usually displaying light cores mantled by very dark or black rims. Thirty-six analyses have been performed in different areas of 33 zircon grains. Analyses distribute in a large Variscan population, three around 570 Ma and the other two at 719 and 965 Ma. The Variscan population is made of 31 analyses among which some of them have a different degree of common-lead, defining a common-lead discordia line with a lower intersection age of 306 ± 3 Ma (Fig. 6b). We interpretate this discordia to be only due to common-lead because points align from the plot in concordia to infinitum. When there is lead-loss, points displaced left and down. In contrast, if the discordance is due to common-lead, points move right and up. When both causes are present, points are never aligned, and one gets just a cloud of points. Nevertheless, we agree that the discordia line in the Fig. 6b is not perfectly defined and, probably one point (the penultimate from concordia) has a small degree of lead-loss added to common-lead. In our experience, black rims rich in U-Th can be metamictic and tend to accumulate non-radioactive lead from surroundings. Rejecting those analyses with a discordance >5%, the remaining 18 plot in a cluster with a weighted mean ²⁰⁶Pb/²³⁸U age of 306 ± 2 Ma (MSWD = 1.0), matching the intersection age, which we consider the age of the crystallization of this rock. Pre-Variscan ages were found in gray restitic cores inside Variscan crystals and entirely restitic grains with oscillatory zoning (Fig. 5b). Predominant Variscan ages were obtained in all other crystals, including the black rims, most of which are discordant and plot along the common-lead discordia (Fig. 6b). U and Th contents, as well as the Th/U ratios, vary considerably depending on the type and area of the zircons. Most Variscan zircons have moderate contents, except the black rims, which are U-rich, from >1000 to 2000 ppm (Suppl. Table S2).

Zircons from the porphyritic monzogranite (SMTM) unit are mainly euhedral, long-prismatic to acicular with short pyramidal terminations, rarely rounded, and have an average size of about 200 µm. In transmitted light, they are pale brown, pinkish, or colorless and always translucent. CL images show a general pattern of quite high cathodoluminescent zircons, with a faint oscillatory zoning or consisting of alternating bands parallel to the C axis (Fig. 5c). Some crystals are surrounded by a black rim, similar to that of sample JAL-16-13 but narrower, so that only one was available for analyses (J162-9.1 in Suppl. Table S2). Twenty-six analyses were performed in 26 crystals, some of them are discordant and not correctable (probably a combination of common lead and lead-loss), so they were rejected for age calculations. The remaining 14 analyses (including that made in a black rim) plot in a cluster yielding a weighted mean ²⁰⁶Pb/²³⁸U age of 305 ± 3 Ma (MSWD = 1.7) (Fig. 6c). U and Th contents and Th/U ratios are very variable, with averages of U = 262 (sd = 260), Th = 273 (sd = 216) and Th/U = 1.3 (sd = 0.5).

Zircons from the marginal leucogranite (VF) are usually euhedral prismatic, even acicular, with short pyramidal forms, and have an average size of >200 µm. In transmitted light, they are pale to dark brown, translucent, or opaque, never colorless. Some of them display transversal healed microfractures. Their CL images show complex crystals mainly composed of cores mantled concordantly or discordantly by thick, very dark, or black rims with no internal structure or complex microstructures, from weak oscillatory zoning and local intermediate resorption to patchy zoning (Fig. 5d). Cores are surrounded or elongated and weakly to strongly resorbed. They are usually medium to high cathodoluminescent with diffuse oscillatory or patchy zoning, unzoned or consisting of alternating bands parallel to the C-axis. Some

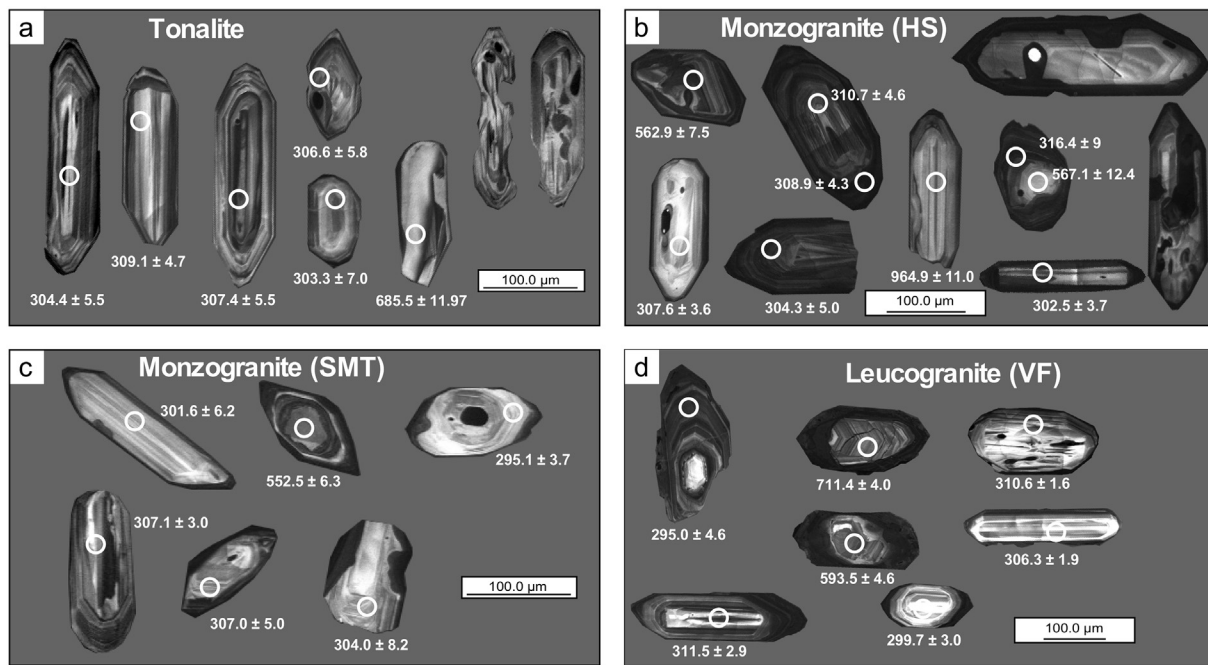


Fig. 5. CL images of representative zircon grains of representative samples from the Jálama pluton with the analyzed spots and concordia ages. (a) tonalite from a microgranular enclave, (b) monzogranite from the HM facies, (c) monzogranite from the HSM facies and (d) leucogranite from the VF facies.

crystals display simpler internal morphologies. Fifty-seven analyses have been performed in different areas of 55 zircon grains: in all morphological types of cores, in homogeneous crystals and, when possible, in black rims. Many of these analyses are moderate to strongly discordant, mainly due to a combination of common-lead and lead-loss. Twenty-two of them had a (no correctible) >10% discordance and were rejected for age calculations. These discordant analyses have been made in black U-rich rims but also in moderate to poor-U cores. The other 35 are concordant or nearly concordant. Among them 9 were made in inherited cores and gave older, from 506 to 841 Ma. The other 26 define a quite large scattered cluster with a weighted mean $^{206}\text{Pb}/^{238}\text{U}$ age of 304 ± 3.5 (MSWD = 5.4) (Fig. 6d). The Variscan zircons have uncorrelated U and Th contents in the ranges of 80–1700 ppm and 17–356 ppm, respectively, with Th/U ratios from 0.01 to 1.6. U and Th contents for inherited zircons are also very variable but better correlated and with Th/U values more restricted, between 0.06 and 0.7 (Suppl. Table S2).

4.2. Zircon O isotopes

Oxygen isotope ratios in zircon depend on $\delta^{18}\text{O}$ of the parent melt and on the $^{18}\text{O}/^{16}\text{O}$ partitioning between melt and zircon. Overall, the JP shows a wide range of $\delta^{18}\text{O}$ (Zrn) values, from ≈ 5.75 to $10.98\text{\textperthousand}$ and an average of $8.96 \pm 1\text{\textperthousand}$ (Suppl. Table S3). The $\delta^{18}\text{O}$ values of all units are higher than uncontaminated mantle values ($5.3 \pm 0.3\text{\textperthousand}$, Valley et al., 1998), and vary in the range of 5.75 – $9.91\text{\textperthousand}$ (average $8.65 \pm 0.856\text{\textperthousand}$) for the tonalitic enclave, 6.04 – $10.98\text{\textperthousand}$ (average $8.95 \pm 1.033\text{\textperthousand}$) for the HS monzogranite, and 7.66 – $10.53\text{\textperthousand} \pm 1.03$ for the SMT monzogranite (average $9.02 \pm 0.9\text{\textperthousand}$). In studied samples, the range of $\delta^{18}\text{O}$ values for xenocrystic cores is very similar to that of magmatic zircons. Some studies indicate that high U concentrations in zircons influence remarkably their U–Pb ages and oxygen isotope ratios (e.g., Gao et al., 2014). However, we have not found significant effects on the U–Pb ages and $\delta^{18}\text{O}$ (Zrn) values. Inasmuch as there is no $\delta^{18}\text{O}$ (Zrn) data for the marginal VF leucogranite, we have used the relation: $\Delta^{18}\text{O}$ (WR-Zrn) ≈ 0.0612 (wt% SiO_2) $- 2.5$ (Lackey et al., 2008; Valley et al.,

2005), which allows $\delta^{18}\text{O}$ (Zrn) values to be calculated based on measured $\delta^{18}\text{O}$ (WR). Accordingly, the $\delta^{18}\text{O}$ values for zircons of the VF leucogranite would be on the order of 10–11‰.

4.3. Sr-Nd-O isotopic data

Representative Sr-Nd-O isotopic data of the JP are presented in Table 3. Initial $^{87}\text{Sr}/^{86}\text{Sr}$ ratios and $\epsilon\text{Nd(t)}$ values have been calculated on the basis of 300 Ma as the average age for the CIZ Variscan magmatism. The $^{87}\text{Sr}/^{86}\text{Sr}$ ratios and $\epsilon\text{Nd(t)}$ values for microgranular enclaves vary from 0.7072 to 0.7112 and -5.75 to -6.10 , respectively, whereas the monzogranites show higher $^{87}\text{Sr}/^{86}\text{Sr}$ ratios (0.7136–0.7260) and $\epsilon\text{Nd(t)}$ values from -5.02 to -5.85 . Overall, the Sr-Nd isotopic compositions overlap with the isotopic compositional range of the S-CIZ metasediments and those of the Spanish Central System granites (Villaseca et al., 1998), but they have lower $\epsilon\text{Nd(t)}$ than the granites from the Central Extremadura batholith and the Castelo Branco pluton (Fig. 7a). The marginal leucogranites show the highest $^{87}\text{Sr}/^{86}\text{Sr}$ ratios (0.8323–0.8695) and $\epsilon\text{Nd(t)}$ of -4.93 and -4.95 . The model ages (TDM) have been inferred from the equation of Liew and Hofmann (1988), ranging from 1330 to 1643 Ma (Table 3). We have not considered the leucogranites because rocks with $^{147}\text{Sm}/^{144}\text{Nd} > 0.165$ yield unreliable Nd model ages (Stern, 2002).

Bulk-rock oxygen isotope ratios for representative samples of the JP are in the range of 9.96–10.52 for the microgranular enclaves and 11.17–12.40 for the granites (Table 3), showing a positive correlation with SiO_2 of the bulk-rock. The higher $\delta^{18}\text{O}$ values for the granites suggest that they were derived from a shallower source than that of the tonalites. In fact, the $\delta^{18}\text{O}$ values of the JP granites are within the range of values reported for the Schist Greywacke Complex (Ugidos et al., 1997) (Fig. 7b). $\delta^{18}\text{O}$ values higher than 10‰ are typical of high- SiO_2 peraluminous granites (Taylor, 1968), and have been reported in several granites from the Central Iberian Zone (Antunes et al., 2008; Martins et al., 2013; Neiva et al., 2011). However, S-type granites from the Spanish Central System have lower values (8.3 to 10.2) (Villaseca et al., 2014).

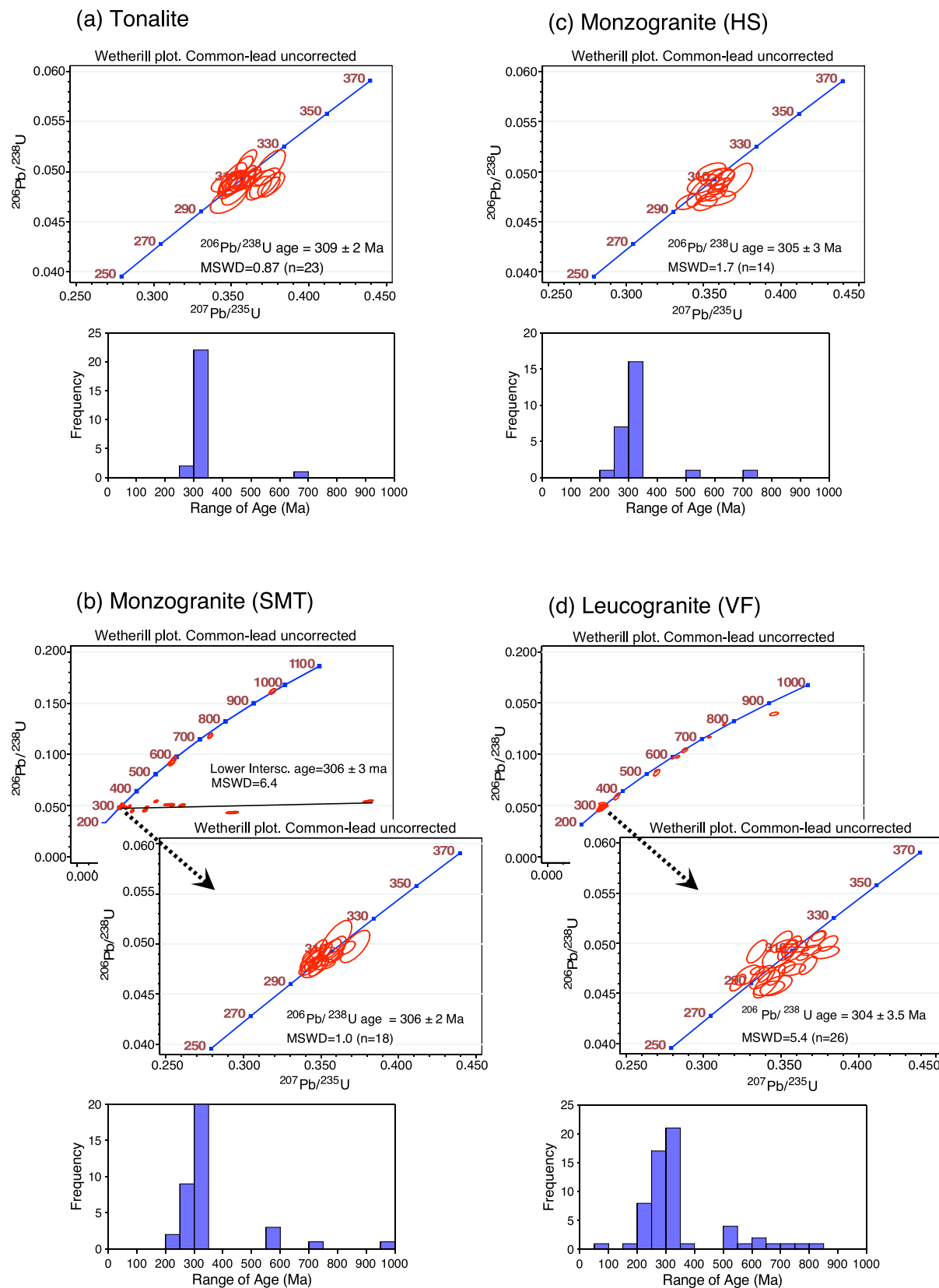


Fig. 6. U—Pb concordia diagrams and histograms for zircons of representative samples from the Jálama pluton. (a) tonalite from a microgranular enclave, (b) monzogranite from the HM facies, (c) monzogranite from the HSM facies and (d) leucogranite from the VF facies.

Table 3

Sr-Nd-O isotopic data for the studied granitic rocks from the Jálama pluton. tDM – two stage crustal residence ages (Liew and Hofmann, 1988).

Sample	Rock type	Rb	Sr	$(^{87}\text{Rb}/^{86}\text{Sr})_m$	$(^{87}\text{Sr}/^{86}\text{Sr})_m$	$(^{87}\text{Sr}/^{86}\text{Sr})_0$	Sm	Nd	Sm/Nd	$(^{147}\text{Sm}/^{144}\text{Nd})_m$	$(^{143}\text{Nd}/^{144}\text{Nd})_m$	$\epsilon(\text{Nd})_{300}$	T_{DM}	$\delta^{18}\text{O}$
JAL-15-26	Tonalite	135	401	0.975	0.711280 ± 08	0.707217	7.81	39.54	0.1980	0.1216	0.5121961 ± 07	-5.75	1492	9.96
JAL-15-10	Granodiorite	197	215	2.659	0.720831 ± 08	0.709480	11.69	61.69	0.1820	0.1048	0.5121532 ± 08	-5.94	1330	10.34
JAL-15-12		187	217	2.498	0.721859 ± 06	0.711196	11.71	58.96	0.1871	0.1129	0.5121612 ± 07	-6.10	1420	10.52
JAL-15-8	Granite HS	376	94	11.730	0.763702 ± 07	0.713624	8.9	55.30	0.1970	0.1196	0.5121871 ± 05	-5.85	1476	11.17
JAL-07-16		298	87	11.104	0.768341 ± 06	0.720936	9.79	48.76	0.2010	0.1244	0.5122037 ± 05	-5.71	1524	11.26
JAL-15-9		391	78	14.499	0.778325 ± 05	0.716429	9.85	49.35	0.1741	0.1198	0.5121924 ± 06	-5.75	1470	11.49
JAL-15-4	Granite SMT	278	83	9.702	0.761249 ± 09	0.719832	9.35	46.50	0.1870	0.1201	0.5121956 ± 08	-5.70	1471	11.32
JAL-15-5		296	64	13.383	0.773248 ± 06	0.716114	6.77	33.87	0.1836	0.1209	0.5121928 ± 07	-5.79	1486	11.35
JAL-07-15		259	88	8.516	0.751701 ± 08	0.715347	5.22	24.39	0.2140	0.1287	0.51222412 ± 07	-5.14	1532	11.46
JAL-15-11		342	32	30.140	0.854712 ± 07	0.726043	2.94	13.18	0.2610	0.1368	0.5122635 ± 06	-5.02	1643	12.00
JAL-15-18	Leucogranite VF	533	28	50.188	1.046604 ± 05	0.832349	1.14	4.10	0.2780	0.1825	0.5123576 ± 05	-4.93	3292	12.26
JAL-12		561	22	70.485	1.170438 ± 06	0.869529	1.27	4.53	0.2803	0.1781	0.5123478 ± 06	-4.95	2974	12.40

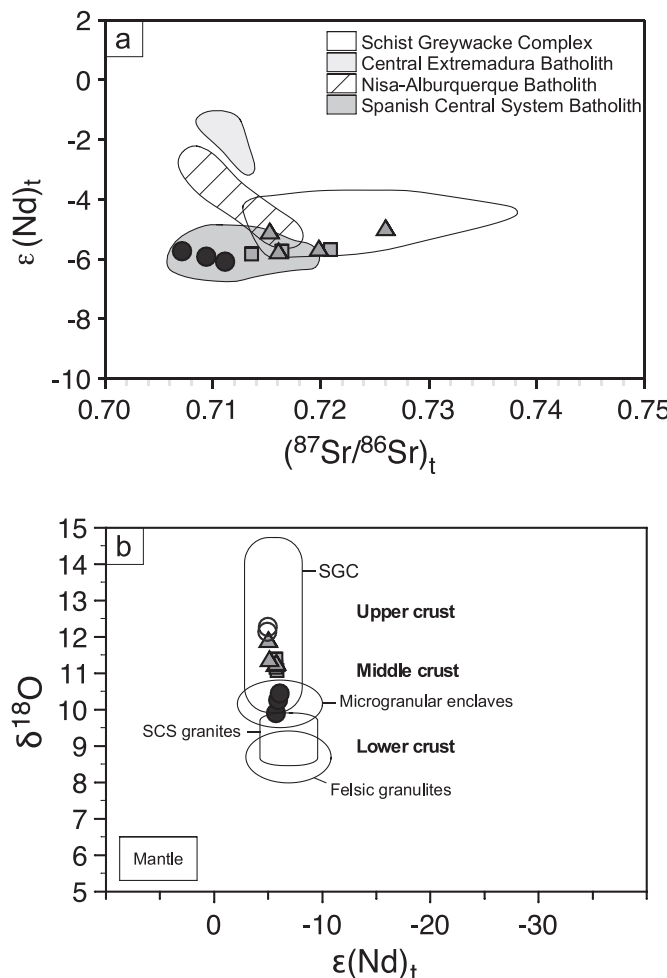


Fig. 7. (a) Initial Sr—Nd composition of granitic rocks from the JP and representative samples of other granites from the Central Extremadura batholith (Antunes et al., 2008; Castro et al., 1999; González-Menéndez and Bea, 2004) and crustal protoliths of the Central Iberian Zone (Beetsma, 1995; Ugidos et al., 1997, 2003; Villaseca et al., 2014). (b) Plot of initial $\epsilon(\text{Nd})_t$ versus $\delta^{18}\text{O}$ values for granitic rocks from the JP. Nd and oxygen isotopic data of the Schist Greywacke Complex (Ugidos et al., 1997), lower crustal xenoliths and mantle are shown for comparison.

4.4. Zircon saturation thermometry

Experimental studies of accessory minerals as zircon and monazite showed that their solubility in melts is strongly sensitive to the temperature and melt composition (Hanchar and Watson, 2003; Montel, 1986).

Zr concentrations at saturation decreases with increases SiO_2 and peraluminosity, and thus lower Zr contents reflect changes in melt composition and lower temperatures. The zircon saturation calculations for JP granitic samples indicate a temperature range of ≈ 640 – 840 °C that decrease with increasing SiO_2 content. The highest temperatures may well correspond to segregated melts, close to the temperatures of partial melting. The relatively low temperatures of some microgranular enclaves, particularly those of tonalitic composition, suggests that they were initially undersaturated in zircon. Initial undersaturation in zircon can be inferred by plotting Zr vs. SiO_2 where Zr initially rises until the inflection point at ≈ 65 wt% SiO_2 (Suppl. Fig. S1), which is interpreted to represent the zircon saturation (Hoskin et al., 2000). LREE saturation temperatures are comparable to those of zircon, and the inflection in La and Ce abundances at ≈ 65 wt% SiO_2 would suggest monazite saturation in the same point as indicated on the Zr- SiO_2 plot.

5. Discussion

5.1. Geochronological constraints on the formation of the granites

Previous geochronological studies on the JP gave contrasting results. Rb-Sr isochron ages of 290 ± 23 Ma and 279 ± 9 Ma were given for the porphyritic monzogranite by Ramírez (1996) and Ruiz et al. (2008), respectively. In addition, Ruiz et al. (2008) attributed a Rb-Sr isochron age for the central unit of 319 ± 10 Ma. However, in the CIZ there is not peraluminous granitoids of the S2 type younger than 300 Ma (Rodríguez-Robles et al., 2018). According to Ramírez (1996) and Ramírez and Grundvig (2000), the JP construction was the result of the emplacement of non-comagmatic successive magma batches generated by partial melting of high-grade peraluminous metamorphic rocks with a large-scale compositional heterogeneity. However, the JP granites have similar U-Pb ages and $\delta^{18}\text{O}$ (Zrn) values (Fig. 6; Suppl. Tables S2 and S3), which are not consistent with a picture of diverse magma sources. Zircon U-Pb ages of granites and tonalite are bracketed in the range of 309–304 Ma. Although the tonalitic enclave appears to be a little older, it is not possible within the analytical uncertainty to establish differences in intrusion ages between the petrographic units that constitute the JP, whereby we can assume that they are coevally formed. In general, the U-Pb ages obtained for the JP overlap to other granites from the southern CIZ; e.g., Castelo Branco pluton (310 Ma), Nisa-Alburquerque (308 Ma), Cabeza de Araya and Trujillo plutons (309 Ma) (Antunes et al., 2008; Gutiérrez-Alonso et al., 2011; Solá et al., 2009). All of them form part of an post-tectonic extensive magmatic event in the southern CIZ, which started at ≈ 310 Ma after the main episodes of collision-driven crustal thickening and the ensuing extensional collapse of the orogen (Valverde-Vaquero et al., 2006).

Apartent Nd crustal residence ages for the JP granites vary between 1.33 and 1.64 Ga, which are akin to those given for other peraluminous granites of the “Serie Mixta” (e.g., Antunes et al., 2008; Castro et al., 1999). Overall, the model ages are comparable to those of other

granitoids of the European Variscides (e.g. Antunes et al., 2008; Janoušek et al., 1995; Kohut and Nabelek, 2008; Martins et al., 2013; Villaseca et al., 1998). The zircons inherited from the granites are mostly Neoproterozoic (≈ 510 – 970 Ma), which is characteristic of materials from the Cadomian orogeny. The JP zircon heritages show a broad overlap with the U–Pb zircon ages reported for the SGC metasedimentary sequence, thus constituting the best candidate to be the source rocks of JP granites.

5.2. Compositional variation

Several different mechanisms have been proposed as responsible for the chemical variation of granitoids; for example: (i) restite unmixing (ii) fractional crystallization; (iii) progressive partial melting (iv) assimilation of crustal rocks and magma-mixing; (v) different sources; (vi) activity of fluids (see Clemens and Stevens, 2012; Clarke, 2019, for an overview), or also a combination of several processes as is the case of the JP. Evidence for open-system processes in the JP is provided by the presence of microgranular enclaves and metasedimentary xenoliths, which preclude simple magmatic differentiation in a closed system. In addition to fractional crystallization, magma mixing, crustal assimilation and activity of fluids are required to account for the compositional variation in the JP. This is supported by the following:

1. Field and petrographic relationships clearly document mixing processes between granitic and tonalitic melts. Local chilled margins and cuspatate contacts are consistent with the magmatic character of the enclaves during their incorporation as magma globules. Moreover, the similar crystallization ages of MME and host granites are not consistent with a restite model for the enclaves, because if they were of restite origin they would be older than the host rocks (Vernon, 2014). Likewise, the presence of acicular apatite, lath-shaped plagioclase crystals, blade-shaped biotite, together with numerous disequilibrium microstructures including quartz rimmed by biotite, mantled feldspars, patchy zoning and cellular morphologies in plagioclases, indicate rapid cooling when more mafic magma (with relatively higher temperature) comes into contact with felsic magma (e.g., Hibbard, 1991). The occurrence of feldspar megacrysts within the MMEs is indicative of the mechanical transfer of crystals during the mixing processes. On the other hand, the occurrence of metasedimentary xenoliths with different degrees of digestion suggests crustal assimilation via syntectic processes during the magmatic ascent (Pesquera et al., 2018).
2. Fractionation of feldspar and biotite could account for much of the variation of Al_2O_3 , TiO_2 , $(\text{FeO} + \text{MgO})\text{CaO}$, K_2O , Rb, Sr and Ba with the increase in SiO_2 . The variation patterns of the K/Rb, Rb/Sr, Nb/Ta and Zr/Hf ratios with increasing SiO_2 reveal an important control of the fractionation processes, chiefly from monzogranites with more than ≈ 71 wt% SiO_2 to VF leucogranites (Suppl. Fig. S1). The K/Rb, Nb/Ta and Zr/Hf ratios show a decrease toward values as low as those of highly evolved magmatic rocks, which have undergone fractional crystallization and interaction of fluids (e.g.; Jahn et al., 2001). The enrichment of lithophilic elements such as Rb, Sn, W, Ta, B, Li and Cs in the JP and other granites of the “Mixed Series” could be related not so much to high fractionation rates but also to the so-called “Geochemical signature of Frauenbach” (Romer et al., 2012). These authors suggest that the strong enrichment of such elements, high initial $^{87}\text{Sr}/^{86}\text{Sr}$, and depletion of Ca, Sr and Ba, as occurs in the Erzgebirge high Rb/Sr granites and other massifs from the European Variscides, reflect the involvement of high Rb/Sr protoliths rather than the result of extreme fractional crystallization alone. Accordingly, they postulate that both Sn-enriched granites of Variscan Europe and metasedimentary rocks with Frauenbach geochemical signatures represent a Gondwana fingerprint. Some late-Variscan granites from the French Central Massif, the Armorican Massif and the CIZ, with more or less depletion in Ca and Sr, together with

high contents in Li, Rb, Sn and high $^{87}\text{Sr}/^{86}\text{Sr}$ values (e.g. Romer et al., 2012; Villaseca et al., 2008), show evidence of the “Frauenbach geochemical signature” inherited from the protoliths. However, although the granitoids of the Mixed Series show similarities with other granitoids from the European Variscides, further investigation is necessary for supporting the above interpretation.

3. The high positive correlation between Zr and REE (Fig. 4) is not consistent with a simple fractionation. Due to zircon crystallization should quickly deplete Zr relative to REEs, the observed correlation can be only established during fractional crystallization if zircon crystallized concomitantly with similar amounts of monazite/xenotime (Muecke and Clarke, 1981). However, the higher amount of REE in phosphates relative to zircon (about 100 to 1000 times that of zircon) means that these minerals do not need to crystallize in similar proportions. The coeval crystallization of these phosphates and zircon would maintain the simultaneous depletion in REE and Zr in the granites without significant changes in their fractionation patterns (Pérez-Soba et al., 2014).
4. A fractional crystallization process to explain the compositional trends defined by the enclaves and host granites is questionable taking into account the following considerations: (i) Field and petrographic observations, in conjunction with major- and trace-elements-based mixing tests, support the formation of granodiorites by mixing tonalites and monzogranites (Pesquera et al., 2018); (ii) The Li, Rb and Cs contents in some granodiorites are relatively high compared to what would be expected if they were part of a differentiation sequence; (iii) Compositional differences between enclaves and host rocks, with discontinuous evolutionary trends on binary variation diagrams; and iv) The lack of cumulus textures in the tonalites, which on the contrary show textures indicative of a rapid crystallization of melts.

5.3. Granitoid sources

The peraluminous granites of the JP, with $A/\text{CNK} \geq 1.1$, low $\text{CaO}/\text{Na}_2\text{O}$ and high $\text{Rb}/\text{Sr}-\text{Rb}/\text{Ba}$ ratios, are consistent with a dominantly metapelitic source. According to Sylvester (1998), lower $\text{CaO}/\text{Na}_2\text{O}$ and higher Rb/Sr , Rb/Ba ratios are characteristic of peraluminous melts derived from plagioclase-poor, clay-rich sources rather than from plagioclase-rich sources. The high P_2O_5 content, which increases with fractionation, are also typical of S-type granitic melts (Chappell, 1999) because the solubility of apatite increases significantly with the aluminum saturation index (Bea et al., 1992; Wolf and London, 1994). Moreover, the behaviour of REE, Y and Th, which show good correlations, is characteristic of granitic rocks derived from metasedimentary sources (Bea, 1996).

High initial $^{87}\text{Sr}/^{86}\text{Sr}$ ratios and low ϵ_{Nd} , as well as high $\delta^{18}\text{O}(\text{WR})$ and $\delta^{18}\text{O}(\text{Zrn})$ values of the JP granites (Table 3; Suppl. Table S3), provide compelling evidence that the JP granites derived from partial melting of crustal material, potentially rocks from the SGC with relatively high P and B levels and similar isotopic values (Fig. 5). Thermal models applied to the CIZ suggest that those parts of the middle crust having enhanced fertility and heat production might have been the source of abundant granite magmatism during a continental collision-related orogeny (Bea et al., 2003).

Unlike the granites, the occurrence of microgranular enclaves of tonalitic composition with a metaluminous affinity might reflect the involvement of mantle-derived mafic melts in the melting processes and possible mixing processes. The participation of the mantle in the genesis of granodiorites, monzogranites and tonalites in the CIZ has already been envisaged by some authors (e.g.; Castro et al., 1999). Intrusions of granodiorites, monzogranites and minor tonalites linked to mantle-derived mafic rocks were attributed to melting of predominantly metaigneous sources in the lower crust (Fernández-Suárez et al., 2011). According to Gutiérrez-Alonso et al. (2011), the mantle upwelling and concomitant melting of lower crust yielded an

upward-migrating thermal anomaly that caused mid-crustal melting and formation of monzogranites and leucogranites.

Notwithstanding these considerations, the lack of exposed mafic rocks in the area of the JP and the fact of their (Sr-Nd-O) isotopic values are near the Sr, Nd and oxygen isotopic compositional range of SGC represents a serious hindrance for a mixing model involving mantle-derived mafic melts. While the granitic rocks with high- $\delta^{18}\text{O}$ values (11.17–12.40, Table 3) and a peraluminous character can be attributed to partial melting of an alumina-rich metasedimentary source, the tonalites require a more mafic source. However, the relatively high initial $^{87}\text{Sr}/^{86}\text{Sr}$ ratio (0.7072), and a Mesoproterozoic two-stage Nd model age (1492 Ma), coupled with negative ε_{Nd} values, crustal Nb/Ta values (12.4), low MgO, Cr, Ni and high Na₂O, K₂O contents, are not consistent with tonalitic magmas being directly evolved from mantle-derived mafic magmas via fractional crystallization. In addition, the oxygen isotope ratio of zircon in the tonalite (average $\delta^{18}\text{O} = 8.65 \pm 0.85$) is much heavier than the zircons derived directly from the mantle ($5.3 \pm 0.6\text{\textperthousand}$; Valley et al., 1998; Bindeman, 2008). Values of $\delta^{18}\text{O}$ in zircon >5.6‰ fingerprint an ^{18}O -enriched crustal component in the magma from which the zircon crystallized (Kemp et al., 2007). Melt-zircon isotopic fractionation varies with melt composition and follows a linear relationship with SiO₂ content (Lackey et al., 2008; Valley et al., 2005). This means that the zircons with an average $\delta^{18}\text{O}$ of $\approx 8.60\text{\textperthousand}$ would be in

equilibrium with a tonalitic melt having $\delta^{18}\text{O} \approx 10\text{\textperthousand}$ for its 60% SiO₂. If we consider a mantle-derived tonalite with a $\delta^{18}\text{O}$ (WR) value of $6.7 \pm 0.3\text{\textperthousand}$ (Lackey et al., 2008), it follows that increasing an uncontaminated tonalite value to the calculated of the JP tonalite requires minimum supracrustal additions of at least 30% of metasedimentary rocks assuming an average $\delta^{18}\text{O}$ (WR) value of $\approx 12.5\text{\textperthousand}$ for SGC (Ugidos et al., 1997), what would mean the tonalite would be largely crustally contaminated.

Experimental studies suggest that dehydration-melting of amphibolites or metabasalts in mid- to lower-crustal levels can yield significant volumes of intermediate partial melts, but very high temperatures (≈ 900 –1000 °C) are needed (e.g. Rapp and Watson, 1995). Zircon saturation thermometry in tonalites from the JP, nevertheless, provides temperatures lower (< 800 °C) than those required, even lower than those of some granodiorites and monzogranites, probably as a result of that magma was initially undersaturated in zircon. Coupled melting of mafic and metasedimentary rocks (Otamendi et al., 2009), and incorporation of recycled felsic material into mafic crustal protoliths to yield intermediate to acid compositions (Kröner et al., 2017) have also been proposed for generation of tonalitic magmas, which would account for the evolved Sr isotopic compositions.

On the other hand, field and petrographic observations, combined with geochemical data and $\delta^{18}\text{O}$ (WR) values of ≈ 10.2 –10.4‰, suggest

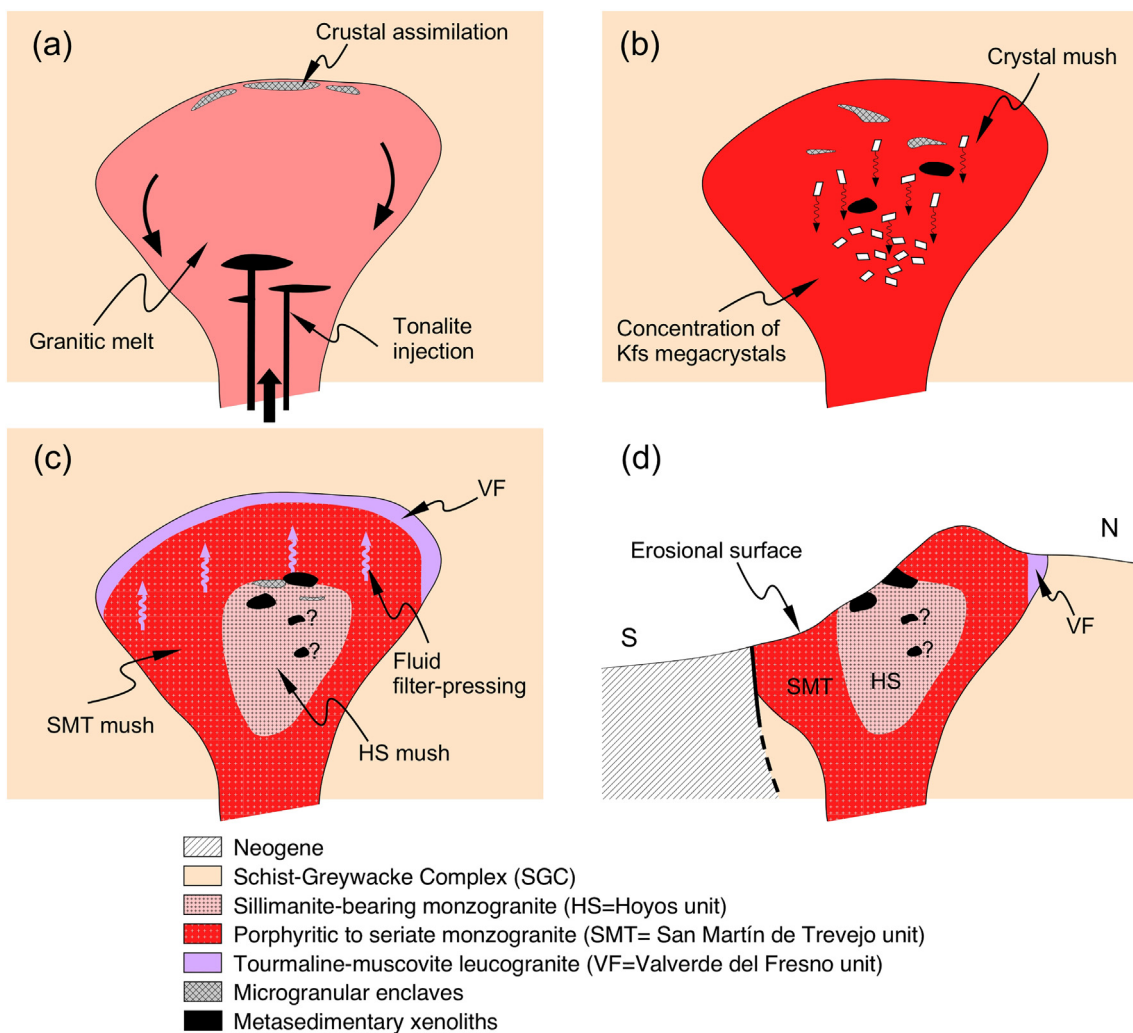


Fig. 8. Schematic diagram (without scale) showing a model of evolution of the Jálama pluton. (a) Formation of the main body by injection of granitic melt and minor amounts of tonalitic melts. (b) Strong interaction between metasedimentary xenoliths, microgranular enclaves and the granitic mush with accumulation of felspars megacrysts in the central part of the pluton. (c) Upward percolation of a more fractionated interstitial melt drawn out from the granite mush, which was assisted by fluid-driven filter pressing. (d) Final stage.

that the granodiorite enclaves are the result of mixing between tonalite and ≈ 15 to 30% of HS monzogranite with $\delta^{18}\text{O}$ (WR) $\approx 11.20\text{\textperthousand}$. This monzogranite was previously contaminated as evidenced from the occurrence of metasedimentary xenoliths. An amount of ≈ 10 –15% of metasedimentary component was estimated to be assimilated by the granitic melt (Pesquera et al., 2018).

5.4. Origin of the reverse Zoning

In contrast to normally zoned plutons with more mafic rims and felsic cores, relatively few reversely zoned intrusions are described in the geological literature (e.g., Allen, 1992; Antunes et al., 2008; Ayuso, 1984; Janoušek et al., 1997; Nabelek et al., 1986). Unlike other granitoids of the "Mixed Series" with normal zonation (eg Cabeza de Araya and Alburquerque, Fig. 1), the JP constitutes an example of reversely zoned intrusion where the most evolved unit outcrops on the periphery of the pluton. Although the Castelo Branco granitoid has been considered as an inversely zoned intrusion (Antunes et al., 2008), it nevertheless presents a more complex zoning in which both the core and the margin include two granites with a similar degree of evolution. The JP does not show marked differences in modal composition between the margin and the centre of the pluton (Fig. 2). Internal zoning in the JP is rather recognized as changes in petrographic characteristics and mineral association. Chemical variations within the major units are more subtle, but the trends of major and trace elements underline an important increase of the fractionation degree from the STM monzogranite to marginal leucogranite of the VF unit.

Excepting the tonalites, it is possible that the JP granites were emplaced as a single magma body, developing an internal zonation that is interpreted as follows (Fig. 8,1) Gravitational instability and bulging of a more hotter portion of the melting front with formation of the main body by injection of granitic melt and minor amounts of tonalitic melts. Assimilation of adjacent metasedimentary rocks is interpreted to be produced during its emplacement, (Fig. 8a). (2) Crystallization grading into granitic mush with concentration of feldspar megacrysts and metasedimentary xenoliths in the central part of the pluton, probably induced by flow differentiation and thermogravitational diffusion, which in turn promote the outward enrichment of fluids. Mingling/mixing between tonalites and the granitic mush took place concurrently with crystallization. Contamination coupled with mingling/mixing processes would be responsible for the lack of systematic compositional gradients within the central units of the pluton (Fig. 8b). (3) Upward percolation of a buoyant interstitial melt drawn out from the granite mush, which was boosted by fluid-driven filter pressing (Sisson and Bacon, 1999); the fluid derived from second boiling (Fig. 8c). Evidence for activity of fluids is provided by the occurrence of miarolitic cavities and pegmatite segregations in leucocratic zones of the SMT unit. The VF leucogranite thus represents a small fraction of melt that formed through fractionation of SMT monzogranite and fluid-filter pressing.

It should be noted, nevertheless, that the relative importance of these processes can not be adequately judged with available data. Structural and gravimetric studies would be necessary to shed light on geometry and emplacement conditions of the pluton.

6. Summary and conclusions

1. The Jálama pluton is a zoned body that intrudes into epizonal domains of the Central Iberian Zone. It consists mainly of a sillimanite-bearing two-mica monzogranite in the central part of the pluton, followed by a tourmaline-bearing two-mica monzogranite, and a muscovite-tourmaline leucogranite on the northern margin of the pluton.
2. At some locations, microgranular enclaves of tonalitic to granodioritic composition occur in monzogranites. Evidence for magma mingling/mixing is provided by field and textural relationships, ruling out the fact that the microgranular enclaves are solid refractory material brought up from the source region. Also, metasedimentary

xenoliths with variable degrees of digestion are relatively common in monzogranites from the central zone, and geochemical data contradict the suggestion that the xenoliths are restitic material.

3. Granitic rocks from the JP are peraluminous, alkali-calcic to calc-alkalic with a ferroan nature. Field and petrographic observations, coupled with geochemical data, document that assimilation and mingling/mixing act in conjunction with fractional crystallization in controlling the compositional evolution of the pluton.
4. The range of 309–304 Ma in zircon ages is interpreted to represent the timescale of formation of the JP, which is believed to have been intruded during post-collisional stage of the Hercynian orogeny.
5. High initial $^{87}\text{Sr}/^{86}\text{Sr}$ ratios, negative $\varepsilon(\text{Nd})_t$ and $\delta^{18}\text{O}(\text{WR})$ data, combined with geochemical data and zircon saturation thermometry, are consistent with a midcrustal origin for the Jálama pluton. Analysis of the oxygen isotope ratios in zircons from granites shows restricted values of $\delta^{18}\text{O}$ (around 9‰) for the magmatic source of the JP, also indicating that the monzogranites of the HS and SMT units have a similar source. Zircon inheritances, together with the metasedimentary character of the source, make the Schist Greywacke Complex the most likely candidate as source rock of the Jálama pluton.
6. The Sr-Nd-O isotopic characteristics of the tonalites preclude a simple crustal or mantle source and therefore it requires further investigation to unravel the origin of these rocks. However, an average $\delta^{18}\text{O}$ (Zrn) value of $\approx 8.65 \pm 0.8\text{\textperthousand}$ for tonalites would indicate a largely contaminated magma with crustal material. Granodiorite can be explained by mixing between tonalitic and granitic melt.
7. The Jálama pluton shows an inverse zonation where the HS unit represents the central zone in which the crustal assimilation effects are chiefly manifested. The marginal VF leucogranite is interpreted to have formed by upward percolation of a small fraction of buoyant interstitial, more evolved melt, which was drawn out from the SMT granitic mush via fluid-driven filter-pressing.

Declaration of Competing Interest

None.

Acknowledgments

This paper has been partially financed by the Spanish Grant CGL2017-84469-P. This is a IBERSIMS publication No. 67. We are indebted to F. Bea for his assistance on zircon oxygen isotope data and U-Pb ages. We also gratefully acknowledge reviews and comments by two anonymous reviewers and thoughtful editorial comments by Xian-Hua Li.

Appendix A. Supplementary data

Supplementary data to this article can be found online at <https://doi.org/10.1016/j.lithos.2021.106002>.

References

- Allen, C.M., 1992. A nested diapir model for the reversely zoned Turtle Pluton, southeastern California. Earth and Environmental Science Transactions of the Royal Society of Edinburgh 83 (1–2), 179–190. <https://doi.org/10.1017/S0263593300007872>.
- Antunes, I.M.H.R., Neiva, A.M.R., Silva, M.M.V.G., Corfu, F., 2008. Geochemistry of S-type granitic rocks from the reversely zoned Castelo Branco pluton (central Portugal). Lithos 103 (3–4), 445–465. <https://doi.org/10.1016/j.lithos.2007.10.003>.
- Ayuso, R.A., 1984. Field Relations, Crystallization, and Petrology of Reversely Zoned Granitic Plutons in the Bottle Lake Complex, Maine. U.S. Geological Survey Professional Paper. 1320 p. 58.
- Bea, F., 1996. Residence of REE, Y, Th and U in granites and crustal protoliths; Implications for the chemistry of crustal melts. Journal of Petrology 37 (3), 521–552. <https://doi.org/10.1093/petrology/37.3.521>.
- Bea, F., 2004. La naturaleza del magmatismo de la Zona Centro Ibérica: consideraciones generales y ensayo de correlación. In: Vera, J.A. (Ed.), Geología de España. SGE-IGME, Madrid, pp. 128–133.

- Bea, F., Fershtater, G.B., Corretgé, L.G., 1992. The geochemistry of phosphorus in granite rocks and the effect of aluminium. *Lithos* 29 (1–2), 43–56. [https://doi.org/10.1016/0024-4937\(92\)90033-U](https://doi.org/10.1016/0024-4937(92)90033-U).
- Bea, F., Montero, P., Zinger, T., 2003. The nature, origin, and thermal influence of the granite source layer of Central Iberia. *Journal of Geology* 111 (5), 579–595. <https://doi.org/10.1086/376767>.
- Beetsma, J.J., 1995. The late Proterozoic/Paleozoic and Hercynian crustal evolution of the Iberian Massif, N Portugal, as traced by geochemistry and Sr-Nd-Pb isotope systematics of pre-Hercynian terrigenous sediments and Hercynian Granitoids. *Tesis Doctoral, Univ. Amsterdam* (223 pp).
- Bindeman, I., 2008. Oxygen isotopes in mantle and crustal magmas as revealed by single crystal analysis. *Reviews in Mineralogy and Geochemistry* 69 (1), 445–478. <https://doi.org/10.2138/rmg.2008.69.12>.
- Black, L.P., Kamo, S.L., Allen, C.M., Aleinikoff, J.N., Davis, D.W., Korsch, R.J., Foudoulis, C., 2003. TEMORA 1: a new zircon standard for Phanerozoic U-Pb geochronology. *Chemical Geology* 200 (1), 155–170. [https://doi.org/10.1016/S0009-2541\(03\)00165-7](https://doi.org/10.1016/S0009-2541(03)00165-7).
- Castro, A., Patiño Douce, A.E., Corretgé, L.G., de la Rosa, J.D., El-Biad, M., El-Hmidi, H., 1999. Origin of peraluminous granites and granodiorites, Iberian massif, Spain: an experimental test of granite petrogenesis. *Contributions to Mineralogy and Petrology* 135 (2–3), 255–276. <https://doi.org/10.1007/s004100050511>.
- Chappell, B.W., 1999. Aluminium saturation in I- and S-type granites and the characterization of fractionated haplogranites. *Lithos* 46 (3), 535–551. [https://doi.org/10.1016/S0024-4937\(98\)00086-3](https://doi.org/10.1016/S0024-4937(98)00086-3).
- Clauqué-Long, J.C., Compston, W., Roberts, J., Fanning, C.M., Berggren, W.A., Kent, D.V., Aubrey, M.-P., Hardenbol, J., 1995. *Two Carboniferous Ages: A Comparison of Shrimp Zircon Dating with Conventional Zircon Ages and $^{40}\text{Ar}/^{39}\text{Ar}$ Analysis, Geochronology, Time Scales and Global Stratigraphic Correlation*. SEPM Society for Sedimentary Geology.
- Clarke, D.B., 2019. The origins of strongly peraluminous granitoid rocks. *The Canadian Mineralogist* 57, 529–550. <https://doi.org/10.3749/canmin.1800075>.
- Clemens, J.D., Stevens, G., 2012. What controls chemical variation in granitic magmas? *Lithos* 134–135, 317–329. <https://doi.org/10.1016/j.lithos.2012.01.001>.
- Corretgé, L.G., Bea, F., Suárez, O., 1985. *Las características geoquímicas del batolito de Cabeza de Araya (Cáceres, España): implicaciones petrogenéticas*. Trabajos de Geología 15, 219–238.
- Corretgé, L.G., Castro, A., García-Moreno, O., 2004. *Granitoides de la Serie Mixta*. In: Vera, J.A. (Ed.), *Geología de España*. SGE-IGME, Madrid, pp. 115–116.
- Díez Balda, M.A., Martínez Catalán, J.R., Ayarza Arribas, P., 1995. Syn-collisional extensional collapse parallel to the orogenic trend in a domain of steep tectonics; the Salamanca detachment zone (Central Iberian Zone, Spain). *Journal of Structural Geology* 17 (2), 163–182. [https://doi.org/10.1016/0191-8141\(94\)E0042-W](https://doi.org/10.1016/0191-8141(94)E0042-W).
- Escuder Viruete, J., Díez Balda, M.A., Rubio Pascual, F.J., González Casado, J.M., Barbero, L., Martínez Poyatos, D., Villar, P., Martínez Catalán, J.R., 2004. *La extensión varisca tardiorrogénica y las deformaciones tardías*. In: Vera, J.A. (Ed.), *Geología de España*. SGE-IGME, Madrid, pp. 87–92.
- Fernández-Suárez, J., Gutiérrez-Alonso, G., Johnston, S.T., Jeffries, T.E., Pastor-Galán, D., Jenner, G.A., Murphy, J.B., 2011. Iberian late-Variscan granitoids: Some considerations on crustal sources and the significance of “mantle extraction ages”. *Lithos* 123 (1–4), 121–132. <https://doi.org/10.1016/j.lithos.2010.09.010>.
- Frost, B.R., Barnes, C.G., Collins, W.J., Arculus, R.J., Ellis, D.J., Frost, C.D., 2001. A geochemical classification for granitic rocks. *Journal of Petrology* 42 (11), 2033–2048. <https://doi.org/10.1093/petrology/42.11.2033>.
- Gao, Y.-Y., Li, X.-H., Griffin, W.L., O'Reilly, S.Y., Wang, Y.-F., 2014. Screening criteria for reliable U-Pb geochronology and oxygen isotope analysis in uranium-rich zircons: A case study from the Suzhou A-type granites, SE China. *Lithos* 192–195, 180–191. <https://doi.org/10.1016/j.lithos.2014.02.002>.
- García de Figuerola, L.C., Martín Herrero, D., Bascones Alvira, L., 1988a. *Mapa Geológico de España*, E: 1:50.000, nº 572 (Valverde del Fresno).
- García de Figuerola, L.C., Rodríguez Alonso, M.D., Bascones Alvira, L., Martín Herrero, D., 1988b. *Mapa Geológico de España*, E: 1:50.000, nº 573 (Gata).
- González-Menéndez, L., Bea, F., 2004. *El batolito de Nisa-Alburquerque*. In: Vera, J.A. (Ed.), *Geología de España*. SGE-IGME, Madrid, pp. 120–122.
- Govindaraju, K., Potts, P.J., Webb, P.C., Watson, J.S., 1994. 1994 report on Whin Sill dolerite WS-E from England and Pitcurrie Micragabbro PM-S from Scotland: Assessment by one hundred and four international laboratories. *Geostandards Newsletter* 18 (2), 211–300. <https://doi.org/10.1111/j.1751-908X.1994.tb00520.x>.
- Gutiérrez-Alonso, G., Fernández-Suárez, J., Jeffries, T.E., Johnston, S.T., Pastor-Galán, D., Murphy, J.B., Franco, M.P., Gonzalo, J.C., 2011. Diachronous post-orogenic magmatism within a developing orocline in Iberia. *European Variscides*. Tectonics 30 (5), 17. <https://doi.org/10.1029/2010TC002845>.
- Hanchar, J.M., Watson, E.B., 2003. Zircon saturation thermometry. In: Hnachar, J.M., Hoskin, P.W.O. (Eds.), *Zircon*. *Reviews in Mineralogy and Geochemistry*. 53, pp. 89–112.
- Hibbard, M.J., 1991. In: Didier, J., Barbarin, B. (Eds.), *Textural anatomy of twelve magma-mixed granitoid systems*, pp. 431–444.
- Hoskin, P.W.O., Kinny, P.D., Wyborn, D., Chappell, B.W., 2000. Identifying accessory mineral saturation during differentiation in granitoid magmas: an integrated approach. *Journal of Petrology* 41 (9), 1365–1396. <https://doi.org/10.1093/petrology/41.9.1365>.
- Ickert, R.B., Hiess, J., Williams, I.S., Holden, P., Ireland, T.R., Lanc, P., Schram, N., Foster, J.J., Clement, S.W., 2008. Determining high precision, in situ, oxygen isotope ratios with a SHRIMP II: Analyses of MPI-DING silicate-glass reference materials and zircon from contrasting granites. *Chemical Geology* 257 (1), 114–. <https://doi.org/10.1016/j.chemgeo.2008.08.024>.
- Jahn, B.-M., Wu, F., Capdevila, R., Martineau, F., Zhao, Z., Wang, Y., 2001. Highly evolved juvenile granites with tetrad REE patterns: the Wuduhe and Baerzhe granites from the Great Xing'an Mountains in NE China. *Lithos* 59 (4), 171–198. [https://doi.org/10.1016/S0024-4937\(01\)00066-4](https://doi.org/10.1016/S0024-4937(01)00066-4).
- Janoušek, V., Rogers, G., Bowes, D.R., 1995. Sr-Nd isotopic constraints on the petrogenesis of the Central Bohemian Pluton, Czech Republic. *Geologische Rundschau* 84 (3), 520–534. <https://doi.org/10.1007/BF00284518>.
- Janoušek, V., Rogers, G., Bowes, D.R., Vaňková, V., 1997. Cryptic trace-element variation as an indicator of reverse zoning in a granitic pluton: the Ríčany granite, Czech Republic. *Journal of the Geological Society, London* 154, 807–815. <https://doi.org/10.1144/gsjgs.154.5.0807>.
- Kemp, A.I.S., Hawkesworth, C.J., Foster, G.L., Paterson, B.A., Woodhead, J.D., Hergt, J.M., Gray, C.M., Whitehouse, M.J., 2007. Magmatic and crustal differentiation history of granitic rocks from Hf-O isotopes in zircon. *Science* 315 (5814), 980–983. <https://doi.org/10.1126/science.1136154>.
- Kohut, M., Nabelek, P.J., 2008. Geochemical and isotopic (Sr, Nd and O) constraints on sources for Variscan granites in the Western Carpathians – implications for crustal structure and tectonics. *Journal of Geosciences* 53 (3–4), 307–322. <https://doi.org/10.3190/jgeosci.033>.
- Kröner, A., Kovach, V., Alexeiev, D., Wang, K.-L., Wong, J., Degtyarev, K., Kozakov, I., 2017. No excessive crustal growth in the Central Asian Orogenic Belt: Further evidence from field relationships and isotopic data. *Gondwana Research* 50, 135–166. <https://doi.org/10.1016/j.gr.2017.04.006>.
- Lackey, J.S., Valley, J.W., Chen, J.H., Stockli, D.F., 2008. Dynamic magma systems, crustal recycling, and alteration in the Central Sierra Nevada Batholith: the oxygen isotope record. *Journal of Petrology* 49 (7), 1397–1426. <https://doi.org/10.1093/petrology/egn030>.
- Le Bas, M.J., Streckeisen, A.L., 1991. *The IUGS systematics of igneous rocks*. *Journal of the Geological Society (London)* 148, 825.
- Liew, T.C., Hofmann, A.W., 1988. Precambrian crustal components, plutonic associations, plate environment of the Hercynian Fold Belt of central Europe: Indications from a Nd and Sr isotopic study. *Contributions to Mineralogy and Petrology* 98 (2), 129–138. <https://doi.org/10.1007/bf00402106>.
- Martínez Catalán, J.R., Rubio Pascual, F.J., Díez Montes, A., Díez Fernández, R., Gómez Barreiro, J., Díaz Da Silva, I., González Clavijo, E., Ayarza, P., Alcock, J.E., 2014. The late Variscan HT/LP metamorphic event in NW and Central Iberia: relationships to crustal thickening, extension, orocline development and crustal evolution. In: Schulmann, K., Catalán, J.R., Martínez, Lardeaux, J.M., Janousek, V., Oggiano, G. (Eds.), *Variscan Orogeny: Extent, Timescale and the Formation of the European Crust*. Geological Society Special Publication, pp. 225–247.
- Martins, H.C.B., Sant'Ovaia, H., Noronha, F., 2013. Late-Variscan emplacement and genesis of the Vieira do Minho composite pluton, Central Iberian Zone: Constraints from U-Pb zircon geochronology, AMS data and Sr-Nd-O isotope geochemistry. *Lithos* 162, 221–235. <https://doi.org/10.1016/j.lithos.2013.01.001>.
- Montel, J.M., 1986. Experimental determination of the solubility of Ce-monazite in $\text{SiO}_2\text{-Al}_2\text{O}_3\text{-K}_2\text{O-Na}_2\text{O}$ melts at 800°C, 2 kbar, under H_2O -saturated conditions. *Geology* 14 (8), 659–662. [https://doi.org/10.1130/0091-7613\(1986\)14<659:EDOTSO>2.0.CO_2](https://doi.org/10.1130/0091-7613(1986)14<659:EDOTSO>2.0.CO_2).
- Montero, P., Bea, F., 1998. Accurate determination of $^{87}\text{Rb}/^{86}\text{Sr}$ and $^{147}\text{Sm}/^{144}\text{Nd}$ ratios by inductively-coupled-plasma mass spectrometry in isotope geoscience: an alternative to isotope dilution analysis. *Analytica Chimica Acta* 358 (3), 227–233. [https://doi.org/10.1016/S0003-2670\(97\)00599-0](https://doi.org/10.1016/S0003-2670(97)00599-0).
- Muecke, G.K., Clarke, D.B., 1981. *Geochemical evolution of the South Mountain Batholith, Nova Scotia: rare-earth-element evidence*. *The Canadian Mineralogist* 19 (1), 133–145.
- Nabelek, P.J., Papike, J.J., Laul, J.C., 1986. The Notch Peak granitic stock, Utah: origin of reverse zoning and petrogenesis. *Journal of Petrology* 27 (5), 1035–1069. <https://doi.org/10.1093/petrology/27.5.1035>.
- Neiva, A.M.R., Silva, P.B., Corfu, F., Ramos, J.M.F., 2011. Sequential melting and fractional crystallization: Granites from Guarda-Sabugal area, central Portugal. *Geochemistry* 71 (3), 227–245. <https://doi.org/10.1016/j.chemer.2011.06.002>.
- Otamendi, J., Dueca, M., Tibaldi, A., Bergantz, G., de la Rosa, J.D., Vujovich, G., 2009. Generation of tonalitic and dioritic magmas by coupled partial melting of gabbroic and metasedimentary rocks within the deep crust of the Famatinian Magmatic Arc, Argentina. *Journal of Petrology* 50. <https://doi.org/10.1093/petrology/egp022>.
- Patiño Douce, A.E., Johnston, A.D., 1991. Phase equilibria and melt productivity in the pelitic system: implications for the origin of peraluminous granitoids and aluminous granulites. *Contributions to Mineralogy and Petrology* 107, 202–218.
- Pereira, M.F., Castro, A., Fernández, C., Rodríguez, C., 2018. Multiple Paleozoic magmatic-orogenic events in the Central Extremadura batholith (Iberian Variscan belt, Spain). *Journal of Iberian Geology* <https://doi.org/10.1007/s41513-018-0063-5>.
- Pereira, M.F., Linnemann, U., Hofmann, M., Chichorro, M., Solá, A.R., Medina, J., Silva, J.B., 2012. The provenance of Late Ediacaran and Early Ordovician siliciclastic rocks in the Southwest Central Iberian Zone: Constraints from detrital zircon data on northern Gondwana margin evolution during the late Neoproterozoic. *Precambrian Research* 192–195, 166–189. <https://doi.org/10.1016/j.precamres.2011.10.019>.
- Pérez-Soba, C., Villaseca, C., Orejana, D., Jeffries, T., 2014. Uranium-rich accessory minerals in the peraluminous and perphosphorous Belvis de Monroy pluton (Iberian Variscan belt). *Contrib. Mineral. Petrol.* 167, 1008. <https://doi.org/10.1007/s00410-014-1008-4>.
- Pesquera, A., Gil-Crespo, P.P., Torres-Ruiz, J., Roda-Robles, E., 2018. Insights into petrogenesis of the Jálama pluton (Central Iberian Zone, western Spain). *International Geology Review* 60 (2), 157–187. <https://doi.org/10.1080/00206814.2017.1316687>.
- Ramírez, J.A., 1996. *Estudio petrológico, geoquímico e isotópico del batolito de Jálama (Norte de Extremadura)*. Ph. D. Thesis, Universidad de Granada (201pp pp).
- Ramírez, J.A., Grundvig, S., 2000. Causes of geochemical diversity in peraluminous granitic plutons: the Jálama pluton, Central-Iberian Zone (Spain and Portugal). *Lithos* 50, 171–190. [https://doi.org/10.1016/S0024-4937\(99\)00047-X](https://doi.org/10.1016/S0024-4937(99)00047-X).
- Rapp, R.P., Watson, E.B., 1995. Dehydration melting of metabasalt at 8–32 kbar: Implications for continental growth and crust-mantle recycling. *Journal of Petrology* 36 (4), 891–931. <https://doi.org/10.1093/petrology/36.4.891>.

- Roda-Robles, E., Villaseca, C., Pesquera, A., Gil-Crespo, P.P., Vieira, R., Lima, A., Garate-Olave, I., 2018. Petrogenetic relationships between Variscan granitoids and Li-(F-P)-rich aplite-pegmaticites in the Central Iberian Zone: Geological and geochemical constraints and implications for other regions from the European Variscides. *Ore Geology Reviews* 95, 408–430. <https://doi.org/10.1016/j.oregeorev.2018.02.027>.
- Romer, R.L., Förster, H.J., Hahne, K., 2012. Strontium isotopes - A persistent tracer for the recycling of Gondwana crust in the Variscan orogen. *Gondwana Research* 22, 262–278. <https://doi.org/10.1016/j.gr.2011.09.005>.
- Ruiz, C., Fernández-Leyva, C., Locutura, J., 2008. Geochemistry, geochronology and mineralisation potential of the granites in the Central Iberian Zone: The Jalama batholith. *Geochemistry* 68 (4), 413–429. <https://doi.org/10.1016/j.chemer.2006.11.001>.
- Sisson, T.W., Bacon, C.R., 1999. Gas-driven filter pressing in magmas. *Geology* 27 (7), 613–616. [https://doi.org/10.1130/0091-7613\(1999\)027<0613:GDFPIM>2.3.CO](https://doi.org/10.1130/0091-7613(1999)027<0613:GDFPIM>2.3.CO).
- Solá, A.R., Neiva, A.M.R., Ribeiro, M.L., 2009. Constraints from granitic plutonism on Paleozoic crustal evolution of the SW Iberian Massif. *Geochimica Et Cosmochimica Acta* 73 (13), A1246.
- Stern, B., 2002. Crustal evolution in the East African Orogen: A neodymium isotopic perspective. *Journal of African Earth Sciences* 34, 109–117. [https://doi.org/10.1016/S0899-5362\(02\)00012-X](https://doi.org/10.1016/S0899-5362(02)00012-X).
- Sylvester, P.J., 1998. Post-collisional strongly peraluminous granites. *Lithos* 45, 29–44. [https://doi.org/10.1016/S0024-4937\(98\)00024-3](https://doi.org/10.1016/S0024-4937(98)00024-3).
- Tanaka, T., Togashi, S., Kamioka, H., Amakawa, H., Kagami, H., Hamamoto, T., Yuhara, M., Orihashi, Y., Yoneda, S., Shimizu, H., Kunimaru, T., Takahashi, K., Yanagi, T., Nakano, T., Fujimaki, H., Shinjo, R., Asahara, Y., Tanimizu, M., Dragusano, C., 2000. JNdI-1: a neodymium isotopic reference in consistency with Lajolla neodymium. *Chemical Geology* 168 (3), 279–281. [https://doi.org/10.1016/S0009-2541\(00\)00198-4](https://doi.org/10.1016/S0009-2541(00)00198-4).
- Taylor, H.P., 1968. The oxygen isotope geochemistry of igneous rocks. *Contributions to Mineralogy and Petrology* 19 (1), 1–71. <https://doi.org/10.1007/BF00371729>.
- Teixeira, R.J.S., Neiva, A.M.R., Gomes, M.E.P., Corfu, F., Cuesta, A., Croudace, I.W., 2012. The role of fractional crystallization in the genesis of early syn-D3 tin-mineralized Variscan two-mica granites from the Carrazeda de Ansiães area, northern Portugal. *Lithos* 153, 177–191. <https://doi.org/10.1016/j.lithos.2012.04.024>.
- Ugidos, J.M., Armenteros, I., Barba, P., Valladares, M.I., Colmenero, J.R., 1997. Geochemistry and petrology of recycled orogen-derived sediments: A case study from Upper Precambrian siliciclastic rocks of the Central Iberian Zone, Iberian Massif, Spain. *Precambrian Research* 84 (3–4), 163–180. [https://doi.org/10.1016/S0301-9268\(97\)00023-5](https://doi.org/10.1016/S0301-9268(97)00023-5).
- Ugidos, J.M., García de Figuerola, L.C., Bascones Alvira, L., Martín Herrero, D., 1984. *Mapa Geológico de España, E. 1:50.000, n° 596 (Moraleja)*.
- Ugidos, J.M., Valladares, M.I., Barba, P., Ellam, R.M., 2003. The Upper Neoproterozoic-Lower Cambrian of the Central Iberian Zone, Spain: chemical and isotopic (Sm-Nd) evidence that the sedimentary succession records an inverted stratigraphy of its source. *Geochimica Et Cosmochimica Acta* 67 (14), 2615–2629. [https://doi.org/10.1016/s0016-7037\(03\)00027-9](https://doi.org/10.1016/s0016-7037(03)00027-9).
- Valley, J.W., Kinny, P.D., Schulze, D.J., Spicuzza, M.J., 1998. Zircon megacrysts from kimberlite: oxygen isotope variability among mantle melts. *Contributions to Mineralogy and Petrology* 133 (1), 1–11. <https://doi.org/10.1007/s00410-005-0432>.
- Valley, J.W., Lackey, J.S., Cavosie, A.J., Clechenko, C.C., Spicuzza, M.J., Basei, M.A.S., Bindeman, I.N., Ferreira, V.P., Sial, A.N., King, E.M., Peck, W.H., Sinha, A.K., Wei, C.S., 2005. 4.4 billion years of crustal maturation: oxygen isotope ratios of magmatic zircon. *Contributions to Mineralogy and Petrology* 150 (6), 561–580. <https://doi.org/10.1007/s00410-005-0025-8>.
- Valverde-Vaquero, P., Díez Balda, M.A., Díez Montes, A., Dörr, W., Escuder Viruete, J., González Clavijo, E., Maluski, H., Rodríguez-Fernández, L.R., Rubio, F., 2006. *Timing of Variscan metamorphism and the Central Iberian paradox. Geophys. Res. Abst. 8, 01309 (European Geosciences Union 2006)*.
- Vernon, R.H., 2014. Microstructures of microgranitoid enclaves and the origin of S-type granitoids. *Australian Journal of Earth Sciences* 61 (2), 227–239. <https://doi.org/10.1080/08120099.2014.886623>.
- Villaseca, C., 2011. On the origin of granite types in the Central Iberian Zone: contribution from integrated U-Pb and Hf isotope studies of zircon. *VIII Congresso Ibérico de Geoquímica*, pp. 271–276.
- Villaseca, C., Barbero, L., Rogers, G., 1998. Crustal origin of Hercynian peraluminous granitic batholiths of central Spain: petrological, geochemical and isotopic (Sr, Nd) constraints. *Lithos* 43 (2), 55–79. [https://doi.org/10.1016/S0024-4937\(98\)00002-4](https://doi.org/10.1016/S0024-4937(98)00002-4).
- Villaseca, C., Merino, E., Oyarzún, R., Orejana, D., Pérez-Soba, C., Chicharro, E., 2014. Contrasting chemical and isotopic signatures from Neoproterozoic metasedimentary rocks in the Central Iberian Zone (Spain) of pre-Variscan Europe: Implications for terrane analysis and Early Ordovician magmatic belts. *Precambrian Research* 245, 131–145. <https://doi.org/10.1016/j.precamres.2014.02.006>.
- Villaseca, C., Pérez-Soba, C., Merino, E., Orejana, D., López-García, J.A., Billstrom, K., 2008. Contrasting crustal sources for peraluminous granites of the segmented Montes de Toledo Batholith (Iberian Variscan Belt). *Journal of Geosciences* 53 (3–4), 263–280. <https://doi.org/10.3190/jgeosci.035>.
- Williams, I.S., Claesson, S., 1987. Isotopic evidence for the Precambrian provenance and Caledonian metamorphism of high grade paragneisses from the Seve Nappes, Scandinavian Caledonides. *Contributions to Mineralogy and Petrology* 97 (2), 205–217. <https://doi.org/10.1007/BF00371240>.
- Wolf, M.B., London, D., 1994. Apatite dissolution into peraluminous haplogranitic melts: an experimental study of solubilities and mechanisms. *Geochimica Et Cosmochimica Acta* 58, 4127–4145. [https://doi.org/10.1016/0016-7037\(94\)90269-0](https://doi.org/10.1016/0016-7037(94)90269-0).